Biological Applications of Perturbed Angular Correlations of γ-Ray Spectroscopy

Lars Hemmingsen,[†] Klára Nárcisz Sas,[‡] and Eva Danielsen*[,§]

QUP, Department of Physics, Technical University of Denmark, Building 309, DK-2800 Lyngby, Denmark, Department of Natural Sciences, Royal Veterinary and Agricultural University, Thorvaldsensvej 40, DK 1871 Frederiksberg C, Denmark, and Nano-Science Center, University of Copenhagen, Universitetsparken 5, DK-2100 København Ø, Denmark

Received January 8, 2004

Contents

* To whom correspondence should be addressed.
[†] Technical University of Denmark.
[‡] Royal Veterinary and Agricultural University.
[§] University of Copenhagen.

1. Introduction

One of the key problems in the biochemistry of metal-containing proteins is to understand how the function of the protein is related to the structure and dynamics of the metal ion binding site. Fundamental questions that may be addressed are, for example: How does the metal ion binding site of an enzyme change during catalysis; how do dynamic processes affect the reaction mechanism; how does the structure of a metal ion binding site depend on the redox state; or how do two redox proteins "recognize" each others redox state? The answers relate directly to enzyme mechanisms and to intermolecular interactions (protein−protein or cell−protein) in metabolic pathways and thus to an understanding of central elements of fundamental processes of life. A large number of techniques for studying such problems exist. In addition to X-ray crystallography and multidimensional NMR that can be used for general protein structure determination, there are a number of metal site specific techniques, of which several are based on the hyperfine interaction of the nucleus with the electric and/or magnetic fields from the electrons and nuclei in the vicinity of the nucleus or with external applied fields. In a hyperfine interaction technique, the interaction between a magnetic field and the magnetic dipole moment of the nucleus or an EFG with the electric quadrupole moment of the nucleus is measured. Examples of such techniques are NMR, NQR, ESR, and Mössbauer spectroscopy. Another such example, with its own particular advantages and limitations, is Perturbed Angular Correlation of γ-rays spectroscopy, usually abbreviated as PAC, or sometimes TDPAC, to stress that the time dependence of the perturbed angular correlation of the γ-rays is measured. The latter technique is the focus of the present work. In this work, we will only discuss the electric nuclear quadrupole interaction (NQI), because it is this term that is normally measured in biological applications of PAC spectroscopy.

10.1021/cr030030v CCC: $48.50
Published on Web 09/08/2004

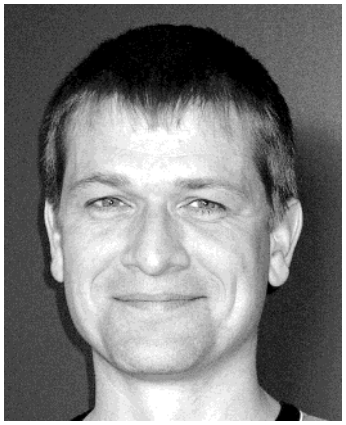

Lars Hemmingsen was born in 1965. He obtained his M.S. in physics from the University of Copenhagen in 1992. From 1992 to 1995, he was a Ph.D. student of R. Bauer at the Royal Veterinary and Agricultural University, working with PAC spectroscopy applied to metal ion-containing proteins and model systems. During his postdoctoral stays, he worked with interpretation of PAC data using quantum mechanical and combined quantum mechanical and molecular mechanical methods at Lund University, Sweden, with U. Ryde and he worked with so-called chemical potential equalization methods and uranyl cation complexes at the Institut de Biologie Structurale, Grenoble, France, with M. J. Field. As an assistant professor and later as a research associate professor at the Royal Veterinary and Agricultural University, he worked with PAC studies of metal ion-containing proteins, peptides, and model systems, as well as the application of theoretical methods to the study of metal ion-containing proteins. In 2003, he moved to the Technical University of Denmark.

Klára Nárcisz Sas was born in Budapest in 1975. She obtained her M.S. in physics from Eötvös University (Budapest) in 2001 with a project on pattern formation in complex systems exemplified by the Liesegang phenomenon and was supervised by Z. Rácz. During her master's studies, she spent one year at The Danish Technical University. She is currently working on a Ph.D. project on electron transport by plastocyanin studied by PAC and is supervised by E. Danielsen.

Eva Danielsen was born in 1962. She obtained her B.S. in physics and mathematics at the University of Århus in 1983, and later, at the same place, she obtained her M.S. in physics with a thesis on the defects in nickel studied by Mössbauer spectroscopy. This work was supervised by G. Weyer. She then took her Ph.D. at the Royal Veterinary and Agricultural University with a thesis on Structure and Dynamics of Proteins and Peptides investigated by PAC, which was supervised by R. Bauer. In 1991, she spent an eight month sabbatical at the University of Maryland at Baltimore in the lab of J. R. Lakowicz where she studied fluorescent anisotropy decays following two-photon excitations. As an assistant professor and later as an associate professor at the Royal Veterinary and Agricultural University, she was involved in developing PAC on studies of copper and zinc proteins and in particular on studies of metal site dynamics. In 2003, she moved to the Nano-Science Center at the University of Copenhagen led by T. Bjørnholm where she is expanding her interest to atomic force microscopy on biological organelles.

This technique is based on radioactive nuclei emitting two or more γ-rays. A property of the nuclear decay is that there is an angular correlation between the two γ-rays, i.e., they are not emitted in random directions with respect to each other. If the nucleus interacts with its surroundings during the decay, the angular correlation is perturbed. This perturbed angular correlation is measured, and it provides a "fingerprint" of the local structure and dynamics.

Several reviews of PAC and compilations of relevant data exist. References to the theory of PAC[1−3] and applications to chemistry, materials science,[4−8] and biology[9,10] can be found in the bibliography.

Since the review by Bauer in 1985,[9] applications related to the biochemistry of metalloproteins have progressed substantially both experimentally and in terms of theoretical interpretations of the experimental data. Furthermore, a large number of successful applications to fundamentally different problems in biological inorganic chemistry have been published in the same period of time. As described in this review, the technique has in the last 1−2 decades expanded to problems such as the structure of the metal ion binding site in a zinc enzyme during substrate conversion (carboxypeptidase); differences in metal ion binding site structure as a function of redox state and the relaxation time upon change of the redox state (blue copper proteins); and use of the method to study interactions between proteins (plastocyanin and photosystem I) and dynamics at metal binding sites (β-lactamase). Experimentally, a much more efficient six detector instrument has been developed and ^{111}Ag has been applied in PAC spectroscopic studies of copper proteins. This isotope is new in biological applications of PAC spectroscopy and has perspectives to make PAC spectroscopy available to a much broader spectrum of researchers. Theoretically, analytic expressions for the perturbation functions have been derived[1,2] and the interpretation of the measured parameters has been improved through quantum mechanical and semiempirical as well as combined quantum mechanical and classical mechanical calculations. The technique has been expanded to include rotational diffusion of the sample molecules in the whole dynamic range, and recently, a new approach has been developed to model dynamic interactions of any origin. In this review, we present an overview of applications of PAC spectroscopy in biology. It is intended as a collection of examples, which provide non-PAC experts insight into the possibilities and limitations of this technique. For the

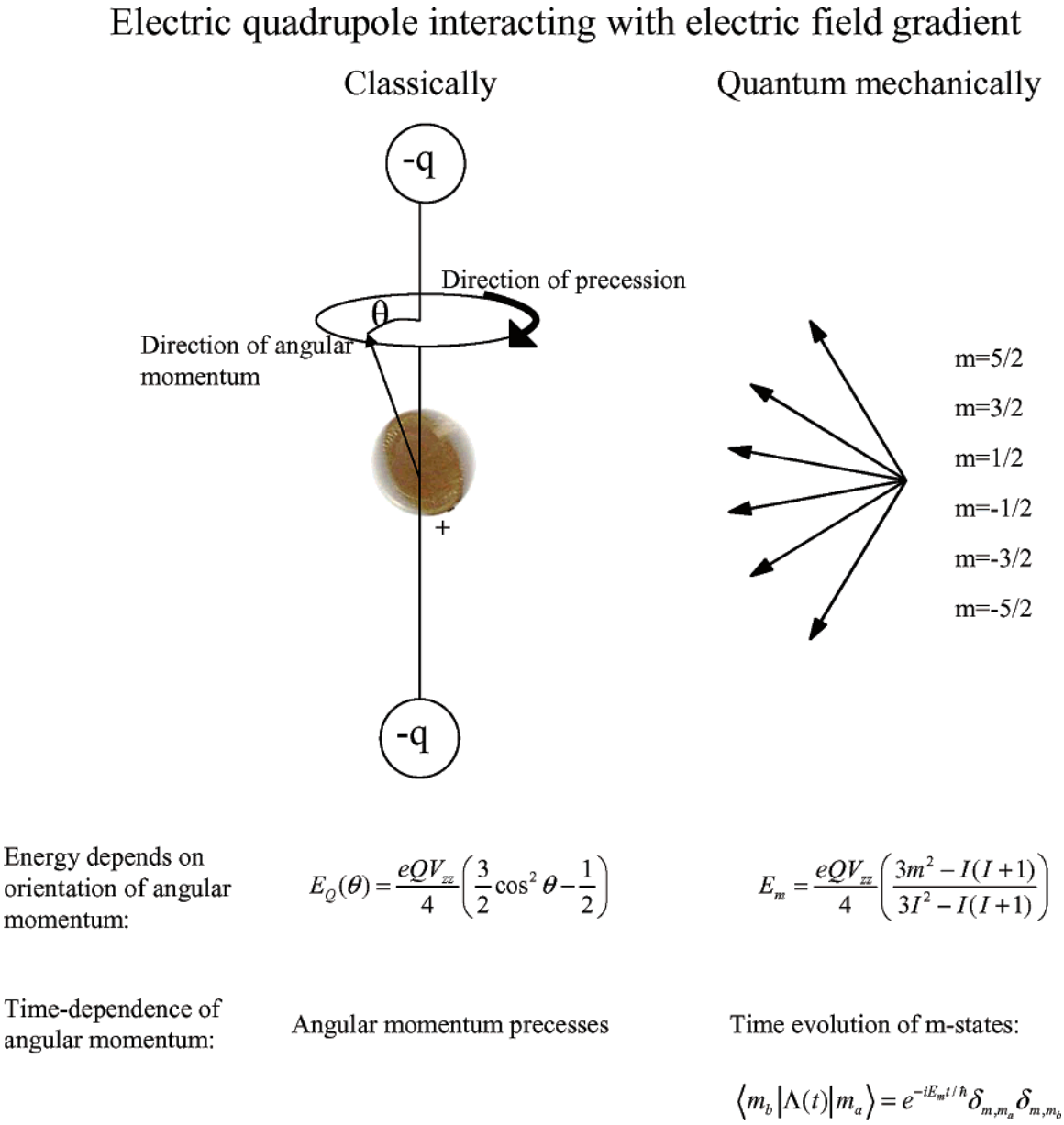

Figure 1. NQI—classical and quantum mechanical description. The most frequent hyperfine interaction measured by PAC spectroscopy on biological samples is the interaction of the electric nuclear quadrupole moment of the nucleus with the EFG from the surrounding charge distribution. This NQI is schematically presented here in a classical and a quantum mechanical representation. In the classical picture, the nucleus is pictured as a charged spinning coin in the field of two external charges (−q). In the figure and the equations, the electric field from the external charges is axially symmetric.

PAC experts as well as nonexperts, it also provides what we have intended to be a complete list of applications of PAC spectroscopy to biologically relevant problems.

2. NQI—A Source for Structural Information

The NQI is the electric interaction of the nonspherical charge distribution of the nucleus (represented by the nuclear quadrupole moment, Q) with the derivative of the electric field (the electric field gradient; EFG) originating from the surrounding charge distribution. The relevant property of the surrounding charge distribution is the traceless part of the EFG, represented by the tensor $\bar{\bar{V}}$. The simplest relevant system is a nucleus bound to two ligands in a linear complex. Before we go into a quantum mechanical treatment of this, it might be helpful to rest shortly on a classical and intuitive picture.

When a spinning charge distribution is placed between two negative charges, the energy of the system depends on the orientation of the angular momentum, i.e., the angle θ. A spinning coin is used to illustrate this and to emphasize that it is a classical picture. The lowest energy is obtained for orientation of the angular momentum along the symmetry axis of the external charge distribution, because this brings the positive charge as close as possible to the negative charges, and the highest energy is obtained for the perpendicular orientation. The expression for the energy, $E_Q(\theta)$, is given in Figure 1. e is the electronic charge, Q is the nuclear electric quadrupole moment, V_{zz} is the zz-component

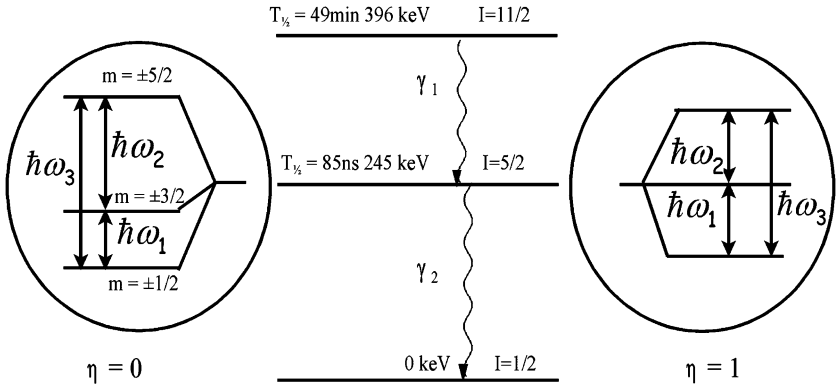

Figure 2. Energy splitting of the PAC relevant nuclear level due to the NQI for ^{111m}Cd. In PAC spectroscopy, the hyperfine splitting of the intermediate nuclear level is measured, in a decay where two γ-rays are emitted successively. For a NQI and an intermediate state of spin I = 5/2, this gives rise to a splitting into three doubly degenerate levels. Middle panel: Schematic presentation of the decay of the 396 keV state of ^{111m}Cd, a widely used PAC isotope in biological applications. Left panel: The energy splitting of the intermediate level in an axially symmetric EFG ($\eta = 0$; $\omega_2 = 2\omega_1$; $\omega_3 = \omega_1 + \omega_2$). Right panel: The energy splitting of an intermediate state in an EFG with maximum asymmetry ($\eta = 1$; $\omega_2 = \omega_1$; $\omega_3 = \omega_1 + \omega_2$).

of the EFG at the position of the spinning coin, and θ is the angle between the axis represented by the external charges (z-axis) and the direction of the angular momentum of the spinning coin. In this simple case of two external charges along the z-axis and the nucleus at the origin of the coordinate system, V_{zz} is given by:

$$V_{zz} = \partial^2\varphi(r)/\partial z^2|_{r=0} - \frac{1}{3}\Delta\varphi = 2k2q/|z_q|^3 \quad (1)$$

where $\varphi(r)$ is the electrostatic potential from the two point charges, Δ is the Laplace operator ($\partial/\partial x^2 + \partial/\partial y^2 + \partial/\partial z^2$), $k = 9 \times 10^9$ Vm/C is the Coulomb constant, and z_q is the z-coordinate of the two point charges each of charge q (assumed to be positioned at the same distance from the nucleus). Note that the V_{zz} decreases with the cube of the distance of the charges from the nucleus. Therefore, PAC spectroscopy is only sensitive to the very local surroundings, typically the coordinating atoms and possible charges within a few Ångströms (first and second coordination sphere). With typical values ($Q = 1$ barn, $q = -e$, $z_q = 2$ Å), the energy difference between $\theta = 0°$ and $\theta = 90°$ is 1.8×10^{-8} eV, that is an extremely small energy difference as compared to the thermal energy, k_BT, of approximately 26 meV at room temperature.

One important point that has not been taken into account in these calculations is that the charge distribution on the cadmium ion is polarized by the point charges. This so-called Sternheimer effect can be very large. For cadmium, the Sternheimer antishielding factor has been calculated by Feiock and Johnson[11] to be −29.3. Taking this into account, the calculated EFG in the example above is 5.3×10^{-7} eV, still much lower than k_BT. The point charge picture is, of course, a highly simplified model of the real cadmium coordination geometry, and more realistic models are described elsewhere in this manuscript.

When the "nucleus" is not oriented along the symmetry axis, a torque is exerted on it. This torque is perpendicular to the angular momentum, and in the classical picture, this leads to a precession of the nucleus, very much like it is often described in NMR.

In the quantum mechanical representation, the orientation of the nuclear angular momentum, I, cannot be in all directions but takes on discrete values of the z-component, given by the magnetic quantum number, m. In the simple case of two external point charges in a linear geometry with the nucleus in the center, this leads to an energy splitting into m substates according to the expression for E_m given in Figure 1. Note that $+m$ and $-m$ give the same energy, due to the m^2 dependency. Therefore, a nucleus with spin 1/2 will not, contrary to the magnetic interaction observed by NMR, experience energy splitting due to the NQI. For a nucleus with spin 5/2, as most frequently used PAC isotopes, three energy levels will result (±1/2, ±3/2, and ±5/2). In the general case of a nonaxially symmetric EFG, the Hamiltonian describing the interaction of the nucleus with the extranuclear field is not diagonal in the m space (see appendix A), but the same number of sublevels will occur. In PAC spectroscopy, this is the energy splitting that is measured, providing a fingerprint of the charge distribution around the PAC isotope (see Figure 2). However, as the simple classical calculation above showed, the splitting is extremely small—so how is it observed? This question will be addressed in the section on PAC.

In general, the external charge distribution is, of course, more complex, and the full traceless part of the EFG tensor, $\bar{\bar{V}}$, is required in the description of the NQI. $\bar{\bar{V}}$ is a 3×3 symmetric and traceless tensor and thus has five independent elements, which can be extracted from a single crystal PAC experiment. For randomly oriented molecules, which is the case in solution, the orientation of the principal axis system with respect to the molecular structure cannot be determined, and only two parameters are necessary to characterize the EFG. One set of parameters is defined by the diagonal elements of the diagonalized EFG, ordered such that $|V_{zz}| \geq |V_{yy}| \geq |V_{xx}|$. The two parameters describing the EFG are

traditionally chosen to be $|V_{zz}|$ and $\eta = (|V_{yy}| - |V_{xx}|)/|V_{zz}|$. The latter is called the asymmetry parameter and runs between 0 (for axially symmetric EFGs; $V_{yy} = V_{xx} = -1/2V_{zz}$) and 1 (for the highest degree of asymmetry; $V_{xx} = 0$ and $V_{yy} = -V_{zz}$).

As a technical note, it should be pointed out that often the EFG, $\bar{\bar{V}}$, is not used in itself, but rather

$$\bar{\bar{\omega}} = \frac{3eQ}{2(3I^2 - I(I+1))\hbar}\bar{\bar{V}}$$

because it includes the nuclear parameters and thus relates more directly to the measured NQI. In that case, the NQI is characterized by $\omega_0 = |\omega_{zz}|$ and η instead of $|V_{zz}|$ and η.

The NQI also has the consequence that the probability of finding the nucleus in state m_b at time, t, given that it was in state m_a at time 0 becomes time-dependent. This is expressed by the time evolution operator $\Lambda(t)$. If $<n|$ denotes the eigenvectors of the Hamiltonian, with eigenvalues E_n, then the matrix elements of the time evolution operator $\Lambda(t)$ are as follows (for time-independent interactions):

$$\langle m_b|\Lambda(t)|m_a\rangle = \sum_n \langle n|m_b\rangle \times e^{-iE_n t/\hbar}\langle n|m_a\rangle \quad (2)$$

It is this time dependence of the transition between m states, which is the quantum mechanical representation of the classical precession of the angular momentum, and it is reflected in the time-dependent perturbation of the angular correlation of the emitted γ-rays; see the following sections.

3. Theory of Perturbed Angular Correlations of γ-Rays

In this section, the theory of PAC of γ-rays is described briefly. A thorough discussion can be found in the review by Frauenfelder and Steffen.[3]

3.1. Angular Correlation of γ-Rays

A γ-ray emitted from a radioactive nucleus carries angular momentum away from the nucleus in the nuclear decay. The total angular momentum is conserved in the nuclear decay, and this is the origin of the angular correlation of γ-rays. The conservation of angular momentum in the nuclear decay puts restrictions on the direction in which the γ-ray is emitted, with respect to the direction of the nuclear spin. At very low temperatures (sub mK), the nuclear spins will orient in the presence of an EFG (or a magnetic field), because the NQI (or magnetic interaction) causes different energies and thus populations of the m sublevels. The γ-rays emitted from an ensemble of oriented nuclei will not be isotropic, due to the conservation of angular momentum. In PAC spectroscopy, however, the nuclear spins are (usually) not oriented by lowering the temperature. Instead, the successive emission of two (or more) γ-rays from a given nucleus is detected. The first γ-ray is detected in a certain sample−detector direction and leaves behind a nucleus with an oriented spin (selecting oriented nuclei by γ-ray detection). Because of the conservation of angular momentum, the second γ-ray is emitted anisotropically with respect to the orientation of the nuclear spin.

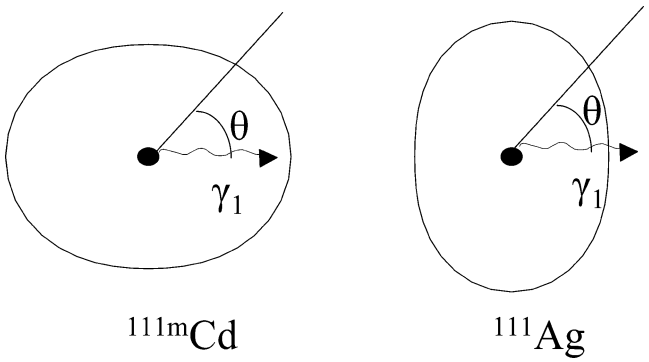

Figure 3. Angular correlation of two γ-rays in the decays of ^{111m}Cd and ^{111}Ag, respectively. The distance from the center to the ellipsoid indicates the relative probability of emission of the second γ-ray (γ_2) at a given angle, θ, with respect to the first γ-ray (γ_1), if γ_1 is emitted as indicated in the figure. For ^{111m}Cd, the second γ-ray is most likely to be emitted in the same or opposite direction, whereas it is least likely to be emitted in the direction perpendicular to the first γ-ray. For ^{111}Ag, it is the opposite.

Therefore, emission of a second γ-ray will be anisotropically distributed with respect to the direction of the first; that is, there is an angular correlation between the two γ-rays. An example is the decay of ^{111m}Cd shown in Figure 2. The distribution of the second γ-ray with respect to the first is a function of the nuclear spin states and the multipolarity of the two γ-rays, and for ^{111m}Cd, the second γ-ray is most likely to be emitted at 180 or 0° with respect to the first, whereas for ^{111}Ag the probability is highest for emission at 90°. This is illustrated in Figure 3.

The idea that γ-rays emitted successively in a nuclear decay are not emitted in random directions with respect to each other was investigated theoretically already in 1940 by Hamilton.[12] The experimental confirmation of angular correlation was performed by Brady and Deutsch in 1947.[13]

If the intermediate nuclear level has spin 5/2, which is the case in almost all used PAC isotopes, the probability density of the second γ-ray being emitted at angle θ with respect to the first and at a time t after the first can be written as:

$$P(\theta,t) \propto e^{-t/\tau}\, W(\theta,t) = e^{-t/\tau}\left[1 + A_2(1)A_2(2)\left(\frac{3}{2}\cos^2\theta - 1/2\right)\right] \quad (3)$$

The exponential decay simply accounts for the lifetime, τ, of the intermediate level. The two amplitudes depend on the nuclear spin states and the multipolarity of the γ-rays, and the amplitude of the anisotropy is given by the product of $A_2(1)$ and $A_2(2)$ denoted A_{22}. Higher order terms containing A_4 have been neglected but are included in appendix A. For the first γ-ray transition from the $I = 3/2$ state to the intermediate state following the β-decay of ^{111}Ag, the amplitude $A_2(1)$ is 0.3742. Because this is positive, it means that the detection of a γ-ray in a certain direction selects an ensemble of nuclei, with the predominant orientation parallel to the emitted

γ-ray. The amplitude of the anisotropy for the second γ-ray from the $I = 5/2$ state to the $I = 1/2$ ground state is -0.5345; thus, the second γ-ray has a higher probability of being emitted at an angle perpendicular to the first than parallel to the first. Calculating the ratio of $W(180,t)$ to $W(90,t)$ for Ag gives 0.73. Thus, the probability of emitting the second γ-ray is 27% lower at 180° than at 90°. For the γ-rays emitted from ^{111m}Cd, the first amplitude is -0.334 and the second is -0.5345; thus, in this case, the angular correlation is positive.

3.2. Perturbed Angular Correlations of γ-Rays

The angular correlation is determined by the properties of the nuclear decay alone and, thus, does not take into account interactions of the nucleus with extranuclear fields. PAC refers to the change in angular correlation between the two γ-rays, due to the interaction of the nucleus with an extranuclear field (hyperfine interaction). This change in anisotropy can be illustrated by the precession of the nucleus described in connection with Figure 1. Thus, as the nuclei precess, the orientation of the nuclear spin changes and consequently the most probable direction of the emission of the second γ-ray changes. Averaging over the whole ensemble, this leads to oscillations in the angular correlation of the γ-rays.

In 1946, Goertzel performed theoretical studies of the effect on the angular correlation when the nucleus interacts with extranuclear fields.[14] The experimental confirmation of this perturbed angular corrleation was performed by Frauenfelder and coworkers in 1951.[15,16] Measuring the perturbation of the angular correlation, it is possible to get information about the EFG produced by the charge distribution around the radioactive nucleus. The EFG is a "fingerprint" of the local electronic and molecular structure around the PAC isotope. The first application of PAC spectroscopy in biology appeared in 1968, when Leipert and co-workers[17] investigated serum albumin using ^{111}In.

In the quantum mechanical formulation, the probability that the second γ-ray is emitted at an angle θ with respect to the first γ-ray, at time, t, after the emission of the first γ-ray, contains terms that are products of the matrix elements of the time evolution operator, $\langle m_b|\Lambda(t)|m_a\rangle$ (see appendix A). Thus, a PAC time spectrum represents interference in the time development between different m states and is therefore not a resonance technique like Mössbauer spectroscopy, ESR, and NMR spectroscopy.

The general expressions can be found in the review by Frauenfelder and Steffen[3] and in the work by Butz.[1,2] Here, we will restrict ourselves to randomly oriented molecules, in which case the perturbed angular correlation becomes:

$$W(\theta,t) = e^{-t/\tau}[1 + A_2(1)A_2(2)G_{22}(t)(3/2\cos^2(\theta) - 1/2)] \quad (4)$$

Thus, the change from the angular correlation appears simply as multiplication by a time-dependent function, $G_{22}(t)$, of the last term in the parenthesis. This means that the perturbation does not change the spatial form of the angular correlation but just makes it change in time. $G_{22}(t)$ is the interesting factor that one wishes to extract from a PAC experiment, because it contains the information about the NQI of the nucleus with it's surroundings and thereby about the coordination geometry.

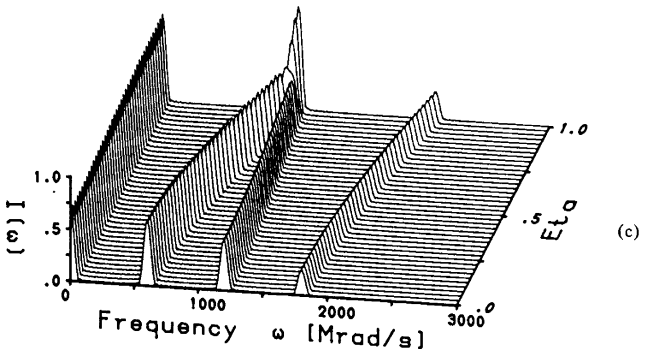

Figure 4. Stacked plot of Fourier-transformed perturbation functions, $G_{22}(t)$, vs asymmetry parameter η for a spin 5/2 intermediate nuclear level. Each energy difference in the hyperfine split intermediate level, see Figure 2, gives rise to a frequency in the PAC spectrum. The frequencies (in this example, $\omega_1 = 600$ Mrad/s, $\omega_2 = 1200$ Mrad/s, and $\omega_3 = 1800$ Mrad/s for $\eta = 0$) and their amplitudes vary as a function of the asymmetry, η, of the EFG.[1] Reprinted with kind permission from ref 1. Copyright 1989 Kluwer Academic Publishers.

For the particular case of a nucleus with an intermediate level of spin 5/2 in randomly oriented but otherwise identical static EFGs, $G_{22}(t)$ contains four terms (see appendix A):

$$G_{22}(t) = a_0 + a_1\cos(\omega_1 t) + a_2\cos(\omega_2 t) + a_3\cos(\omega_3 t) \quad (5)$$

The three frequencies, ω_i, each correspond to an energy difference as illustrated in Figure 2, and they and the four amplitudes, a_i, depend on η and ω_0 in a known manner. This functionality can be found in the general paper by Butz[1,2] or in the review by Bauer.[9] The dependence of a_i and ω_i on η is illustrated in Figure 4. It is noteworthy that not only the transition frequencies, ω_i, but also the amplitudes, a_i, provide information about the NQI. For example, the amplitudes must have magnitudes such that $a_1 \geq a_2 > a_3$. So, if an experiment gives, for example, $a_2 \geq a_1$, it is a clear indication that more than one NQI and thus more than one coordination geometry is present. This particular case is observed for the complex of alcohol dehydrogenase with its coenzyme NADH.[18]

The equation above gives the answer to the question posed in the section on the NQI: The extremely small energy differences between the m sublevels are $\hbar\omega_i$ and are extracted as oscillations of the angular correlation between the two γ-rays! The angular frequency corresponding to the energy difference, $\Delta E = \hbar\omega$, of the example below eq 1, where two elementary charges are placed at a distance of 2 Å, gives an ω of 27 Mrad/s = 0.027 rad/ns = 0.027 Grad/s. Including the Sternheimer antishielding factor for Cd of -29.3[11] changes ω to 791 Mrad/s. For comparison, model calculations applied to a linear complex of two

cysteines and a cadmium ion predict an ω of 600 Mrad/s (vide infra).

3.3. Time-Dependent Interactions: A Source of Information on Dynamics of Biomolecules

The equations above hold for static NQIs. If, however, the EFG changes in the time between the emissions of the two γ-rays, the equations have to be modified. This can be the case if the molecules are undergoing rotational diffusion due to Brownian motion in the sample, but it can also be the case if the molecules are not rigid but change conformation or undergo other dynamic processes in the time between the two γ-rays. Examples exploring both situations will be given below.

Although the molecule of interest can be immobilized by freezing, precipitation, or adsorption, it is also possible to carry out experiments in solution. We will therefore briefly describe the effect of rotational diffusion. The rotational diffusion is described by the rotational correlation time τ_c, which for a spherical molecule depends on the viscosity (ξ), the temperature (T), and the volume of the molecule (V): $\tau_c = V \cdot \xi/(T \cdot k_B)$,[19] where k_B is Boltzmanns constant. For slow reorientation, the function $G_{22}(t)$ becomes exponentially damped by the factor $\exp(-t/\tau_c)$. This corresponds to a slow loss of phase coherence of the precessing nuclei due to the slow reorientation of the molecule. In the fast limit, the perturbation function becomes $G_{22}(t) = \exp[-2.8\omega_0^2\tau_c(1 + \eta^2/3)t]$. In the intermediate range, no analytic expressions exist, but the function can be calculated as described by Danielsen and Bauer[20] or simulated as described by Danielsen et al.[21] An example of how rotational diffusion affects the perturbation functions, $G_{22}(t)$, is given in Figure 5. Usually, PAC experiments on proteins in solution are carried out with sucrose added typically to 55 W/W % and at 1° C, to slow the rotational diffusion of the molecules.

As it will be discussed for plastocyanin, carboxypeptidase, and β-lactamase below, it is also possible to monitor the effect of internal motion or dynamics at the metal ion binding site in the protein. The effect on the PAC spectrum depends on the time-scale of motion. As with many other techniques, one observes motional narrowing when the transition between a number of states becomes fast enough. For slow motion, the PAC spectrum will reflect the "snapshot" distribution of structures—whether this is a number of discretely different conformations—or a continuous distribution of conformations, e.g., a Gaussian distribution due to small differences in conformation from one molecule to another.

It is possible to determine rate constants for chemical exchange of the PAC isotope in analogy with chemical exchange in NMR but at a shorter time scale. In the simple case of exchange between two sites, A and B, both with lifetime τ with $\omega_0 = \omega_A$ and $\omega_0 = \omega_B$ respectively, which both have axially symmetric EFGs ($\eta = 0$) and the same symmetry axis, the problem can be solved analytically.[23,24] In this case, the spectroscopic signals for both sites are resolved when $\tau \gg 1/(\omega_A - \omega_B)$, damping of the signal

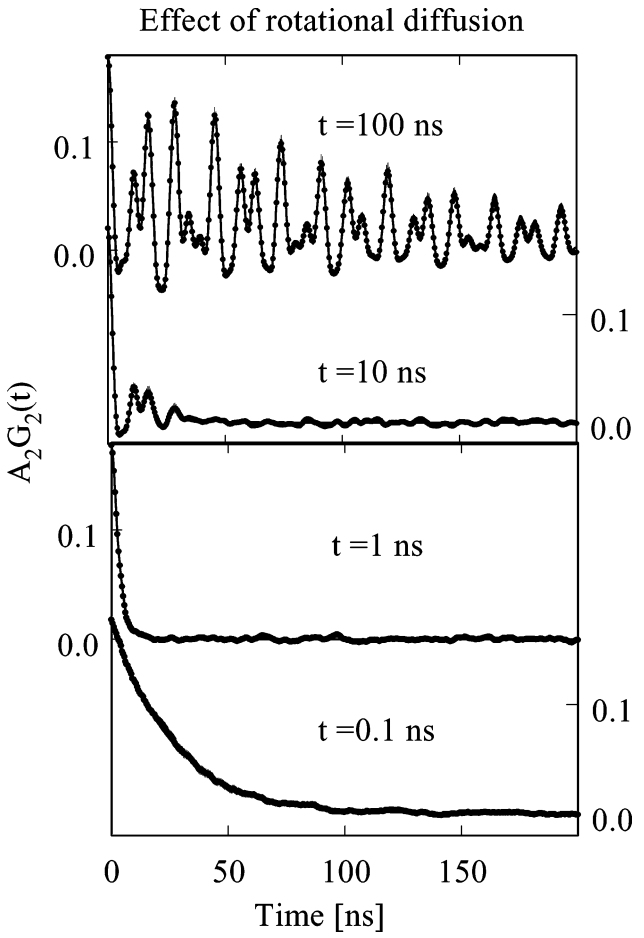

Figure 5. Effect of time-dependent interactions on the perturbation function. Here, the effect of rotational diffusion is shown. The figures show the perturbation function, $A_{22}G_{22}(t)$, for ^{111m}Cd, simulated with the PAC simulator.[22] The lifetime of the random process causing the reorientation varies from 100 to 0.1 ns. The other parameters of the simulation were as follows: $\omega_0 = 0.354$ rad/ns and $\eta = 0.435$, corresponding to parameters from a PAC experiment on cadmium-substituted azurin. For further details, see ref 21. For slow rotational diffusion, the reorientation leads to an exponential damping of the perturbation function of the static interaction. For fast rotational diffusion, the nuclei lose phase coherence, and the perturbation function becomes a simple exponential decay. Reprinted with permission from ref 21. Copyright 2002 Kluwer Academic Publishers.

is strongest for $\tau = 2/(\omega_A - \omega_B)$, and one sharp weighted average signal appears for $\tau \ll 1/(\omega_A - \omega_B)$. A more general derivation, based on perturbation theory,[25] gives a similar behavior of the spectral line shapes. In this particular example, the eigenfunctions of the Hamiltonian do not change. This is not generally the case since a change of the orientation of the principal axis system of the EFG or a change in the value of η will both change the eigenfunctions of the Hamiltonian. This complicates the treatment of the problem significantly and also leads to a decay of the so-called "hardcore term" symbolized by a_0 in eq 5. For ^{111m}Cd, typical frequency differences are 100 Mrad/s, giving maximal damping of the signals for exchange occurring at a time scale of 20 ns. The difference in frequencies can be as low as about 1 Mrad/s, limited by the resolution of the spectrometer, and up to about 500 Mrad/s, limited by the naturally

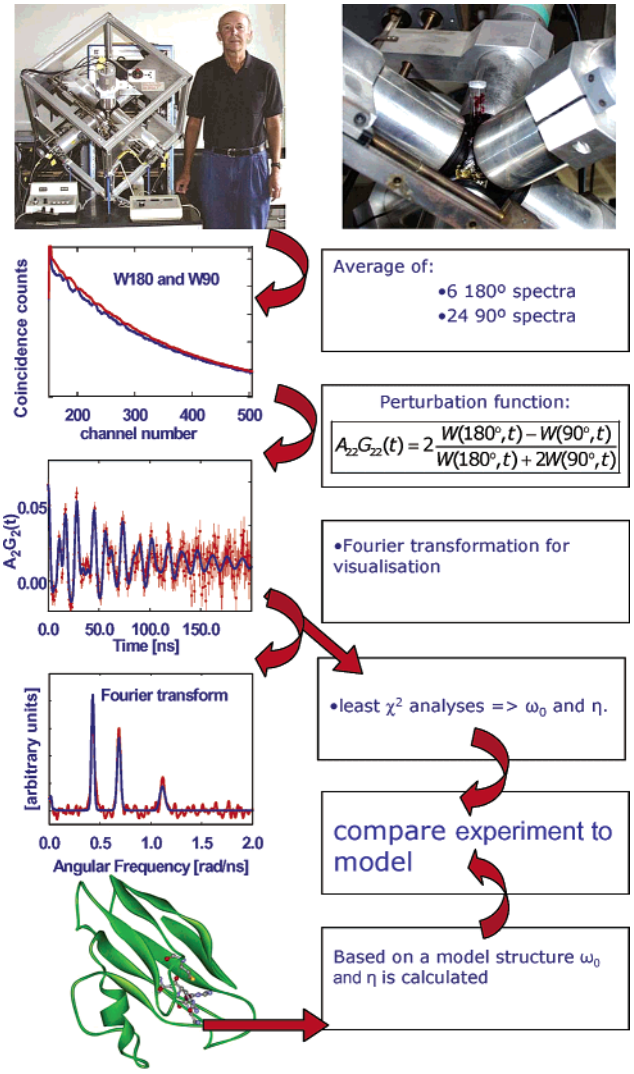

Figure 6. PAC spectroscopy in a nutshell—from data acquisition to data interpretation. Top: Six detector instrument with a sample in a test tube. Next, the "raw" PAC data where the two γ-rays have been detected in detectors at right angles (24 possible combinations of two detectors) or with 180° (six possible combinations of two detectors) between them. Note that $W(180°, t)$ and $W(90°, t)$ oscillate as a function of time, on top of the exponential decay. These oscillations contain the information of interest in PAC spectroscopy, and in the next panel, this information is extracted in the perturbation function, $A_{22}G_{22}(t)$. For visualization, a cosine Fourier transformation is usually carried out. The three frequencies in this example correspond to ω_1, ω_2, and ω_3 in Figure 2. The functional form of the perturbation function is known from the theory of PAC, eq 5, and the parameters in the function are fitted to the experimental data.

occurring NQI strengths for ^{111m}Cd. An example of chemical exchange in PAC spectroscopy can be found in the section on carboxypeptidase.

3.4. PAC Instrument and Data Collection

The typical "state of the art" PAC instrument is described by Butz et al.[26] It consists of six BaF_2 scintillation detectors with conical fronts arranged at right angles to each other; see Figure 6. BaF_2 is chosen due to the need of optimizing both time resolution and energy resolution. The instrument at the Royal Veterinary and Agricultural University has a time resolution of about 850 ps full width at half-maximum at the energies of ^{111m}Cd.[27] For each pair of detectors, $W(\theta,t)$ is collected (see, for example, ref 5). As the detectors are positioned at right angles to each other, θ is either 90 or 180°. $W(\theta,t)$ will contain a background due to accidental coincidences of γ_1 and γ_2 that needs to be subtracted before the geometrical average of all six 180° spectra, named $W(180°,t)$, and of all 24 90° spectra, named $W(90°,t)$, are formed. The reason for using the geometrical average is that the detector efficiencies cancel when the $A_{22}G_{22}(t)$ [$= A_2(1)A_2(2)G_{22}(t)$] is formed in the following way:

$$A_{22}G_{22}(t) = 2\frac{W(180°,t) - W(90°,t)}{W(180°,t) + 2W(90°,t)} \qquad (6)$$

Usually, $A_{22}G_{22}(t)$ is Fourier transformed for easier visualization of the comparison of the data to model functions. The data are analyzed by least χ^2 analysis, where the data are approximated by the function:

$$A_{22}G_{22}(t) = B_0 + A_{22}^{\text{eff}} \sum_i f^i G^i_{22}(\omega_0,\eta,\Delta\omega_0/\omega_0,\tau_c) \qquad (7)$$

where B_0 represents a constant background and the index, i, in the sum runs over the number of different coordination geometries present in the sample. The meaning of the different parameters is summarized in the following section.

In the instrument at the laboratory at the Royal Veterinary and Agricultural University in Copenhagen, Denmark, shown in Figure 6, the sample can be inserted into the center in an ordinary test tube, and the temperature can be controlled between −20 and +45 °C. The distance from the sample to the detectors is regulated automatically continuously during a measurement, to keep the highest feasible count rate without saturating the detectors.

3.5. Parameters Used for Analysis of PAC Data

The perturbation function, $A_{22}G_{22}(t)$, is fitted with five parameters: A_{22}^{eff}, η, ω_0, $\Delta\omega_0/\omega_0$, and τ_c. The physical significance of these parameters is summarized in this section.

The meaning of η and ω_0 has already been described in the section about the NQI. Thus, ω_0 gives an indication of the strength of the interaction, and η is always between zero and unity in magnitude, with $\eta = 0$ corresponding to axial symmetry ($V_{xx} = V_{yy}$) around the z-axis. η and ω_0 depend on the coordination geometry of the metal ion and can be calculated, if the ligands and their positions are known, either by using a semiempirical method developed for cadmium[28] or first principle quantum mechanical[29] methods. In a single crystal experiment, that is for nonrandomly oriented molecules, it is further possible to determine the orientation of the principal axis coordinate system of the EFG tensor.[30]

The measured amplitude of the anisotropy, A_{22}^{eff}, depends on nuclear properties and on the geometry of the experimental setup. For the experimental six detector setup used at the Royal Veterinary and

Agricultural University in Copenhagen, Denmark, with the detectors as close as possible to a 1 mL sample, it is about 0.06 for ^{111m}Cd while the maximum experimentally observed value is 0.16.[31] The reason for the lower value in the setup used at our laboratory is the fact that the sample is not a point source and the detectors are covering an angle that is not infinitesimally small. Thereby, the angular correlation is averaged over the actual sizes of the sample and the detectors, and the maximum value is not achieved. For longer sample−detector distances and a smaller sample volume, a higher value is obtained, because the geometry of the setup becomes more ideal. For a given sample−detector geometry, A_{22}^{eff} is a constant, and it is a useful test when analyzing the data that this value must be found. If the value obtained by the least χ^2 analysis is significantly smaller than this constant, the data analysis must be extended. Possible reasons for this can be coordination geometries or dynamics that are not accounted for.

As described above, Brownian motion causes a change in the orientation of the EFG for a given nucleus while it is in its intermediate energy level. This is taken into account by fitting the parameter τ_c, which is the rotational correlation time of the molecule.[20]

Small differences in the coordination geometry from molecule to molecule are normally described by a Gaussian frequency distribution centered at ω_0, with width $\Delta\omega_0/\omega_0$. A relatively small $\Delta\omega_0/\omega_0$ indicates a very well-defined, rigid coordination geometry. A relatively large $\Delta\omega_0/\omega_0$ represents a coordination geometry with several accessible structures on the conformational energy surface, i.e., a flexible structure. This way of analyzing the distribution of conformations assumes that η is identical for all of the molecules, and it shows up in the spectra as a line broadening where the relative line width is the same for all (three) lines. When this is not the case, such as in the example of plastocyanin in a following section, it is sometimes more informative to describe the frequency distribution as a distribution in the $\omega_{yy} - \omega_{zz}$ plane, where ω_{yy} and ω_{zz} are the two numerically largest eigenvalues of the NQI tensor.[32]

If more than one NQI is present in a PAC measurement, each of them is fitted with the set of parameters described above, with the effective amplitude shared between the NQIs according to the population of the different structures. This is here parametrized by the relative fraction, f_i, where $\sum f_i = 1$.

It is important to ensure that the site of interest is the one that is populated by the radioactive isotope, since unwanted populations give poorer statistics to the one of interest but also make the data analysis more complicated since each new population introduces five new parameters. How this is ensured depends on the problem under investigation, but in general, it is important that the radioactive isotope is well-separated from the substance that it was activated in. For example, for ^{111m}Cd and ^{111}Ag the isotopes are usually produced in a Pd matrix from which they have to be purified (see ref 33 for the production of ^{111}Ag and ref 10 for the production of ^{111m}Cd). If significant amounts of palladium are left, they may compete with the PAC isotope in binding to the metal ion binding site of interest and thus give rise to unbound or unspecifically bound metal ions of the PAC isotope. Equally important is it that the sample is pure, so that the PAC isotope does not bind to other proteins. For multimetal proteins, it is often possible to vary the population of the different metal ion binding sites by varying the stoichiometry or adding "cold" (nonradioactive) metal ions before the PAC isotope is added. A special cause for multiple components is the after effects following electron capture (EC) decays. These might show up as additional components reflecting that the isotope after the EC is located in a distribution of structures caused by the after effect (an example of this is given by Bauer et al.[34]).

3.6. Theoretical Interpretations of PAC Data

The cadmium ion, Cd(II), as well as the cadmium atom have spherically symmetric electronic wave functions, $4d^{10}5s^05p^0$ and $4d^{10}5s^25p^0$, respectively, and therefore no EFG at the site of the cadmium nucleus. In complexes, the EFG is consequently produced either by bonding between cadmium and ligands or by point charges and their polarizing effect on the electrons of cadmium. In the past 10−15 years, it has become possible to perform reasonably accurate first principle calculations of EFGs. In fact, several nuclear quadrupole moments for light nuclei are now derived from measured NQIs and ab initio quantum chemical calculations of EFGs.[35] Also, for heavier nuclei, several studies have been performed (refs 29 and 36 and references therein). However, only very few of these investigations are related to biochemically interesting systems, since their large size makes it very resource demanding to treat them quantum mechanically. A promising approach seems to be combined quantum mechanical and classical mechanical calculations, where the interesting part of the system is treated quantum mechanically and the rest is treated by molecular mechanics.[37] This is particularly useful in relation to calculations of EFGs because they reflect the (very) local charge distribution, as the EFG operator falls off with the cube of the distance from the PAC nucleus. For systems in the crystalline state, the density functional approach of K. Schwarz and P. Blaha[38,39] (and references therein) has provided a number of very interesting results.

For cadmium, a semiempirical molecular orbital method was developed by Bauer et al.[28,31] with the particular aim of interpreting PAC experiments on biological systems. The method has proven reliable, and it is much faster, about a factor of 10^7 for a typical cadmium complex, than first principle calculations. From eight test cases (six of which are proteins), a standard deviation of 27 Mrad/s for the diagonal elements of the NQI tensor (0.15 au for the eigenvalues of the EFG tensor) was found for this method (see appendix B). In addition to this, tests have been performed using ab initio calculations as

Table 1. Characteristic Parameters for Isotopes Appearing in Table 3[121]

parent	half-life	decay	isomer	half-life (ns)	$E(\gamma_1)$ (keV)	$E(\gamma_2)$ (keV)
^{62}Zn	9.186(13) h	EC/β^+	^{62}Cu	4.57(18)	596.56(13)	40.84(3)
^{99}Mo	65.94(1) h	β^-	^{99}Tc	3.61(7)	739.50(2)	181.0939(19)
^{111m}Cd	48.54(5) min	IT	^{111}Cd	85.0(7)	150.82(2)	245.42(1)
^{111}In	2.8049(1) days	EC	^{111}Cd	85.0(7)	171.28(3)	245.42(1)
^{111}Ag	7.45(1) days	β^-	^{111}Cd	85.0(7)	96.73(8)	245.42(1)
^{133}Ba	10.52(13) years	EC	^{133}Cs	6.27(2)	356.017(2)	80.997(2)
^{160}Tb	72.3(2) days	β^-	^{160}Dy	2.02(1)	197.0352(10), 879.383(3), 1177.962(4), 1271.880(8)	86.7882(4)
^{181}Hf	42.39(6) days	β^-	^{181}Ta	10.8(1)	133.024(17)	482.182(23)
^{199m}Hg	42.6(2) min	IT	^{199}Hg	2.45(2)	374.1(1)	158.37950(9)
^{204m}Pb	67.2(3) min	IT	^{204}Pb	265(10)	911.78(7)	374.72(7)
isotopes that have only been used for the sum-peak method						
^{147}Nd	10.98(1) days	β^-	^{147}Pm	2.50(5)	439.895(22)	91.10(2)
^{152}Eu	13.542(10) years	EC	^{152}Sm	1.428(7)	841.586(8)	121.7825(4)

references, and in most cases, good agreement was found. For a more detailed discussion, see refs 29 and 40. The semiempirical method has been successfully applied in several of the references in the bibliography. In connection with the example of the blue copper proteins, a model calculation is worked out in detail as an illustration of how it can be applied. An easy to use JAVA-based program exists on the web for calculations using the semiempirical method.[41] The assumptions in the semiempirical method are described in appendix B. On the basis of the assumptions in the model and the large impact this model has had on the interpretation of PAC data from Cd complexes, the authors suggest naming this model BASIL for Bauers Axially Symmetric Independent Ligands model.

3.7. Available Isotopes

Some characteristic parameters of PAC isotopes are listed in Table 1. A more complete list of isotopes can be found in the review by Rinneberg.[5] In general, the data are easiest to interpret when the isotope has an isomeric excited state, i.e., only γ-rays are emitted. However, for isotopes that have so far been used for biological work, isotopes with isomeric excited states are limited to ^{111m}Cd, ^{204m}Pb, and ^{199m}Hg, which all have rather short half-lives, of the order of 1 h. This means that the production facility has to be close to the experimental setup and that the time available for radiochemistry and metal substitution of the proteins is limited. In the case of ^{111m}Cd, which is often used in biological applications, the isotope can be produced by α-bombardment of ^{108}Pd. This is done at a cyclotron facility at the National Hospital about 10 min drive from the laboratory that we have been using. The transport and the radiochemical separation take about 2 h in total, leaving a strong enough source for 2−3 good PAC experiments. For details of the cadmium production and separation, see ref 18.

For nonisomeric states, the spectra can be affected by so-called after effects. The least problematic of these is in the β-decays, where the charge of the nucleus increases by 1+. Haas and Shirley have studied the effect of the β-decay for ^{111}Ag, ^{117}Cd, and ^{181}Hf and found well-defined field gradients for 80−90% of the nuclei formed.[4] This indicates that the nuclei occupy the site of the parent and that the electronic charge distribution relaxes on a time scale much shorter than the lifetime of the PAC isotope. As described in the sections below on Ag-azurin and Ag-plastocyanin, the change of charge can however also be used to study dynamics of the structure, related to biologically relevant conformational changes for redox active metal ions, e.g., in electron transport. EC decays are often dominated by strong after effects. The hole left by the electronic capture is filled by electronic transitions that often result in the emission of Auger electrons leaving the daughter in a highly charged state. This gives severe problems with the data interpretation, for example, for the decay of ^{111}In as compared to ^{111m}Cd.[34]

In addition to the lifetime of the parent isotope and the nature of the decay, another important parameter is the lifetime of the intermediate state. To the best of our knowledge, the isotopes used so far for time differential PAC spectroscopy all have half-lives of the intermediate state between 2 ns and 1 μs. The lower limit is largely given by the time resolution of the electronics, but even with unlimited time resolution, the lifetime of the intermediate state has to be long enough for one oscillation in $A_{22}G_{22}(t)$ to take place. The upper limit is related to the probability of observing accidental coincidences between γ_1 and γ_2. The longer the lifetime is, the lower the source strength has to be kept in order to keep the ratio of accidental to true coincidences low, but the lower source strength limits the statistical accuracy.

Many applications of PAC spectroscopy to biological problems are carried out with metal ions that are different from the native metal ion in the biological system. Exceptions are the mercury studies of MerA mentioned in section 4.3.2 and the molybdenum-containing proteins described in section 4.3.4.2. However, in many cases, Cd, Ag, or Hg is used to study zinc or copper proteins. Therefore, special care must be taken in the interpretation of the data. The information obtained might only be valid for the metal ion-substituted protein and not for the wild type. For cadmium-substituted zinc enzymes, the enzymatic activity can be checked. This is often conserved, although not fully, as in the example of carboxypeptidase mentioned in section 4.2.2, or the activity profile can be shifted as a function of pH, as in the example of carbonic anhydrase (section 4.2.3). For copper ion-containing proteins, the situation is

more complicated. Substitution of copper with cadmium, silver, or mercury does not conserve the redox activity. On the other hand, substitution with the monovalent or divalent metal ions also has the advantage of catching the protein in the different oxidation states. This allows studies of the interaction of the copper protein to its redox partner in different redox states. Special information can be obtained by comparing PAC spectra of Cd- and Ag-substituted or Cd- and Hg-substituted proteins, because this gives important information about the rigidity of the metal ion binding site and which differences in conformation are energetically favored as discussed in section 4.1.1.1.

3.8. TIPAC/Sum-Peak Method

If the statistical accuracy or the time resolution is insufficient to monitor the time differential PAC spectrum, it is still sometimes possible to gain information from the TIPAC spectrum. This can for example be the case if the time evolution of the sample is to be followed, and it has been used to gain information on different in vivo processes. Experimentally this can sometimes simply be done by integrating the individual $W(\theta,t)$ spectra before the ratio is formed

$$A_{22}\overline{G_{22}(t)} = 2\frac{\overline{W(180°,t)} - \overline{W(90°,t)}}{\overline{W(180°,t)} + 2\overline{W(90°,t)}} \qquad (8)$$

Thus, the time-integrated perturbation factor is the weighted average:

$$\bar{G}_{22} = \frac{1}{\tau_N}\int_0^\infty e^{-t/\tau_N} G_{22}(t)\,\mathrm{d}t \qquad (9)$$

where τ_N is the lifetime of the radioactive nucleus in the intermediate state. When the time differential correlation is studied, a short time resolution as compared to the nuclear lifetime is required, whereas by the time-integrated correlation method a time resolution that is equal to the nuclear lifetime is sufficient. The form of $G_{22}(t)$ and the value of $\bar{G}_{22}$ depend on the rotational correlation time τ_c and on the magnitude of the NQI in the intermediate state.

One useful application of the time-integrated perturbation factor is the study of time developments. If a spectrum recorded at the beginning of an experiment differs from a spectrum recorded later, it is possible to follow the time development of the sample by measuring the time-integrated perturbation factor.

A special version of TIPAC is the sum-peak method. The sum-peak occurs when two γ-rays fall on the detector within its time resolution and are counted as one with a total energy corresponding to the sum of the energies of the two γ-rays. From the intensity of the sum-peak relative to the intensity of the two individual peaks, the time-integrated perturbation factor can be determined.[42] The advantage is that the method can be applied for isotopes with very short half-life times of the intermediate state and with only one detector. The disadvantage is of course that the time-integrated attenuation factor depends on the rotational correlation time as well as η and ω_0, making it difficult to interpret changes of the attenuation factor.

4. Examples of Biological Applications of PAC Spectroscopy

In the following section, we have chosen some of the biological applications that we find particularly interesting. The order of the examples has been chosen such that zinc- and copper ion-containing proteins and other applications are separated. We have chosen the role of methionine in blue copper proteins as the first example. In this problem, the structural use of the method is introduced on a very simple but much debated biochemical problem. In the next example of plastocyanin, the focus is more on the dynamics, both internal motion and the use of PAC spectroscopy, to study protein−protein interactions via changes in rotational diffusion. From there, we move on to the multicopper proteins. For the zinc ion-containing proteins, we have chosen to focus on the recent work on β-lactamase, where combining the methods of NMR and PAC spectroscopy has been important for identifying the time scale of dynamics at the metal ion binding sites. In carboxypeptidase, it has been possible to measure the actively converting enzyme as well as different physical states of the sample (solution and crystalline). Alcohol dehydrogenase has been investigated in a number of PAC studies, and we have chosen to show the spectral changes with pH, as a typical application. The transferrins are included as one of the most detailed biological applications of PAC spectroscopy; then, PAC spectroscopy as a tool for studies of radiation damage on DNA is discussed; and finally, some interesting examples of in vivo studies and oriented samples are included, to illustrate the diversity of the method. We hope that the detailed examples in combination with the much more complete list of examples in the following tables will provide the reader with an impression of what PAC spectroscopy can be used for, how it works, and some of the pitfalls.

4.1. Copper Ion-Containing Proteins

4.1.1. Blue Copper Proteins

Blue copper proteins provide an excellent starting point for examples of applications of PAC spectroscopy, because a number of investigations exist that show how PAC spectroscopy can be used as a method for studying protein−protein interactions as well as metal site structure and dynamics.

4.1.1.1. Structure of Metal Ion Binding Site in Blue Copper Proteins. Azurin, stellacyanin, amicyanin, and plastocyanin all belong to the family of blue copper proteins. These proteins are involved in electron transfer processes, and as a natural consequence of their function, they are all small proteins of about 10 kDa molecular mass. They are characterized by their strong blue color in the oxidized state caused by an intense absorbance (3−6 mM^{-1} cm^{-1}) at 590−630 nm. The characteristic metal ion binding site in blue copper proteins is denoted as a type 1

copper site, and in this type of copper site, the Cu(II) ion is coordinated to two histidines and one cysteine in an almost planar configuration. Perpendicular to this plane, a methionine is often found (see Figure 7). The role of this axial methinonine has been debated, since the distance from the copper ion to the sulfur of the methionine is larger than a normal bonding distance [3.1 Å for Cu(II)-azurin].[43]

The role of the methionine was the issue of the first ^{111m}Cd PAC study on blue copper proteins.[27] In this study, wild-type azurin of *Pseudomonas aeruginosa* and Met121X mutants of azurin (*P. aeruginosa* and *Alcaligenes denitrificans*) were compared to stellacyanin (*Rhus vernicifera)*, where the methinonine is naturally replaced by a glutamine in the amino acid sequence. This was later expanded by a PAC study using ^{111}Ag on wild-type azurin as well as Met121Leu-azurin of *P. aeruginosa*.[33] In Figure 8, the Fourier-transformed PAC spectra of Ag-azurin, Cd-azurin, Ag-Met121Leu-azurin, and Cd-Met121Leu-azurin are compared. A comparison clearly shows that for wild-type azurin metal substitution with Ag or Cd results in almost the same structure. This structure is conserved for Ag-azurin when Met121 is substituted by a leucine, but for the cadmium-substituted mutant, the NQI separates into two almost equally populated coordination geometries of which only one is similar to wild-type azurin. The other form appears as broad peaks in the Fourier transform at frequencies of about 0.35, 0.50, and 0.85 rad/ns.

The interplay between metal ion binding site structure and metal ion was further studied by comparison of PAC spectra on ^{199m}Hg-substituted azurin (*P. aeruginosa*), stellacyanin (*R. vernicifera*), and plastocyanin (*Spinacea*).[45] These studies also support that methionine does not take part in bonding to the metal but appears to stabilize the metal ion binding site geometry. The fact that the NQIs of the ^{111m}Cd and ^{199m}Hg derivatives of all the type 1 copper proteins scale by the same scaling factor indicate that the geometry is predetermined by the peptide conformation.

4.1.1.2. Comparison of Model Calculations and Experiments. The experiments on Met121Leu-azurin indicate that the methionine does not coordinate because there are no major differences between the Ag wild-type and mutant proteins. This is further supported by comparing the experimental data with model calculations on different metal ion binding site structures; see Figure 8: A three-coordinated 2His, Cys structure, a four-coordinated structure including the methionine, and a five-coordinated structure with Gly45 as an additional ligand. A comparison of the spectra of azurin with the calculated spectra clearly shows that the measured spectra are in best accordance with the structure where the assumed ligands are the two histidines and the cysteine. An example of model calculation using the BASIL model can be found in appendix C.

Because methionine does not seem to coordinate but on the other hand is a conserved residue, the question remains what the role of the axial methionine is. Part of an explanation can be found in observing the changes that occur when methionine

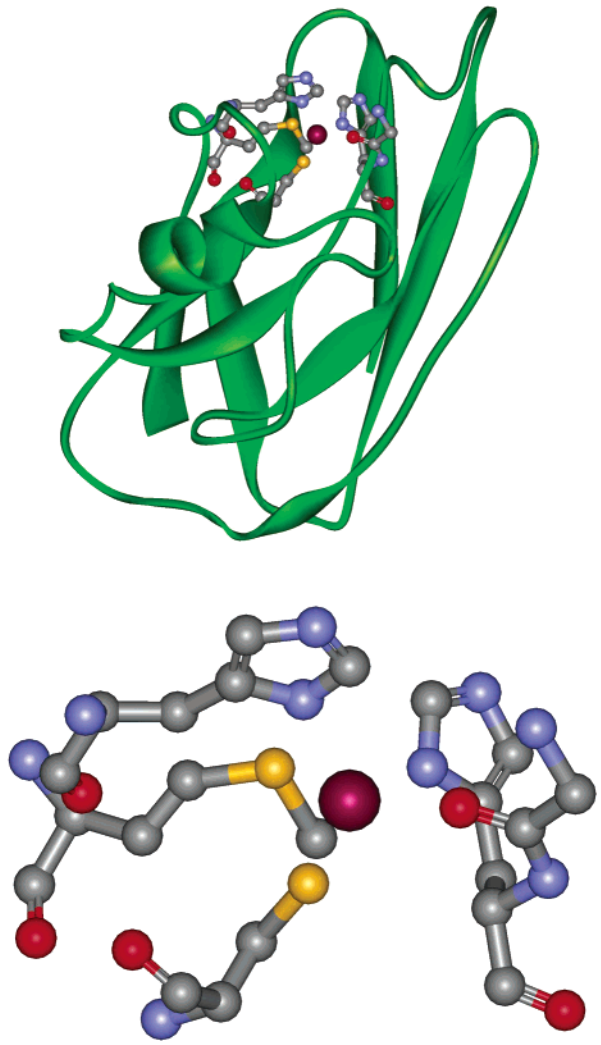

Figure 7. Metal ion binding site of *P. aeruginosa* azurin (PDB file 1AZU[44]). A typical type 1 metal ion binding site of a copper protein is characterized by coordination to a cysteine and two histidines. In most cases, there is an axial methionine at a distance of about 3 Å from the copper ion. It was shown by PAC spectroscopy that the methionine does not coordinate to cadmium or silver. However, in the mutant proteins where the methionine has been substituted by a leucine or an alanine, it seems that a water molecule may coordinate to the metal ion. Thus, one function of the methionine might be to prevent a water molecule from entering the metal ion binding site.[27,33]

121 is substituted by the amino acids Asn, Asp, Gln, Ala, Leu, and Glu.[27] All substitutions gave rise to significant changes in the spectra for the Cd-substituted proteins. In the case of the noncoordinating amino acids, leucine and alanine substitution gave rise to two different NQIs, both present in the sample, of which one has a NQI similar to wild-type azurin. The other is interpreted as a coordinating water ligand. These data together with other observations using other techniques suggest that one role of the axial methionine is not to coordinate to the metal ion but rather to create an environment where it is not possible for water to enter. Because a water molecule in this case would be more likely to bind to the metal ion in the divalent case than in the monovalent case, this would change the redox potential as well as the reorganization energy. That the

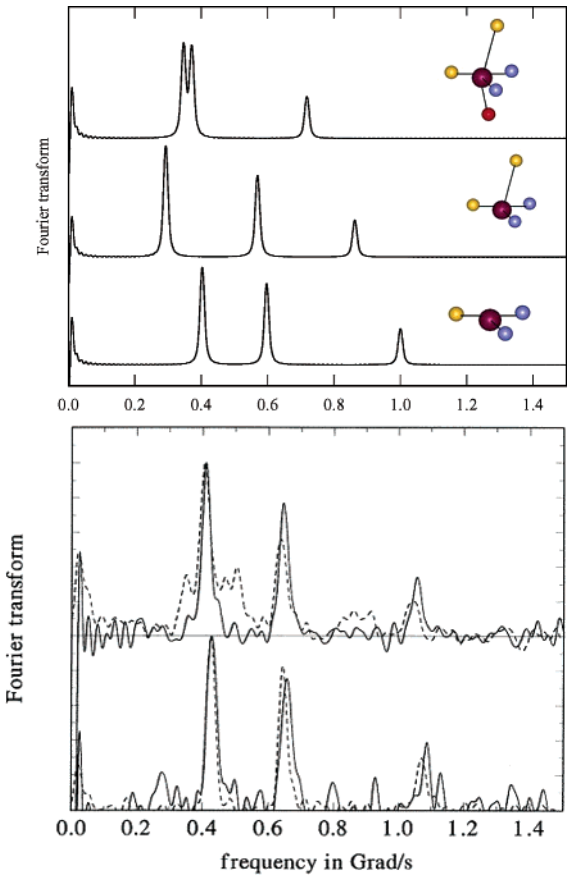

Figure 8. PAC studies on *P. aeruginosa* azurin. Lower panel: The lower spectra are recorded for the wild type, and the upper spectra are recorded for the Met121Leu mutant.[33] Dashed line ^{111m}Cd and solid line ^{111}Ag PAC spectra. Upper panel: Calculated spectra assuming 3-, 4-, or 5-coordination. The model calculation that comes closest to the observed data is the structure where only the three, in plane, ligands coordinate. The spectra of the wild type for the two metal ions are very similar, indicating that the structure is essentially the same. For the Cd-substituted Met121Leu mutant, however, additional broad peaks appear (around 0.35, 0.50, and 0.85 Grad/s), indicating that an additional coordination geometry has appeared. PAC spectra from ^{111}Ag have negative amplitudes in the Fourier transform and have been multiplied by −1 in order to make a comparison with the Fourier transforms for ^{111m}Cd easier. The lower panel is reprinted with permission from ref 33. Copyright 1997 American Chemical Society.

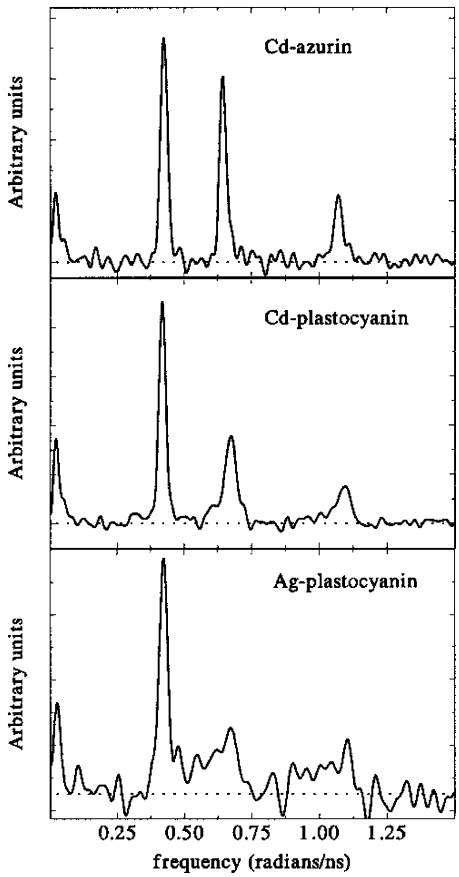

Figure 9. PAC spectra of spinach plastocyanin indicate dynamics at the metal ion binding site. Top panel: Fourier transform of the perturbation function of Cd-azurin. Middle panel: Fourier transform of the Cd-plastocyanin perturbation function. Bottom panel: Fourier transform of ^{111}Ag-plastocyanin perturbation function. All three spectra were collected at 1 °C in 55% w/w sucrose. Note that the first peak is almost identical for all three spectra but that the second and third peaks are slightly shifted and broadened for the plastocyanin spectra. For ^{111}Ag, this shift depends on the time window used in the Fourier transform, such that the lines are shifted to lower frequencies for data collected immediately after the decay from Ag to Cd. The dotted horizontal lines represent 0. Reprinted with permission from ref 47. Copyright 1999 American Chemical Society.

methionine does not take part in bonding to the metal but appears to stabilize the metal geometry was also supported by ^{199m}Hg studies of azurin.[45,46] For references to studies of other mutants of azurin, please refer to Table 3.

4.1.1.3. Plastocyanin: Dynamic Change of Coordination Geometry. Figure 9 shows the PAC spectrum of Ag-plastocyanin and Cd-plastocyanin from spinach as compared to Cd-azurin (*P. aeruginosa*). It is clear that the general features are the same as for azurin, and the data are also interpreted as coordination to the cysteine and the two histidines. A closer inspection, however, reveals an unusual broadening of the lines in the Fourier transform for plastocyanin.[47,49] An analysis of the spectra showed that this unusual line broadening was best described by a constant ω_{yy} of 0.2532(2) rad/ns and an ω_{zz} of 0.3484(4) rad/ns with a relative Gaussian distribution of 2.8%. Theoretical considerations similar to those in appendix C show that moving the histidines in the metal-His-His-Cys plane will change the value of ω_{zz} and leave ω_{yy} unchanged. On the basis of this, the ^{111m}Cd PAC data were interpreted as in-plane motion of one of the histidines; see Figure 10. This is even more pronounced, but in a different way, when one inspects the ^{111}Ag spectra of plastocyanin. For Ag-plastocyanin, the positions of the second and third frequency depend on which part of the perturbation function is used in the Fourier transform; that is, the Fourier transform of the early part (0−17 ns) is different from the Fourier transform of the later part (17−169 ns). For windows that are close to the time of the emission of the first γ-ray, the second and third peaks are shifted to lower frequencies, whereas at later times they are positioned as for ^{111m}Cd-plastocyanin. To understand this, one must inspect the decay of ^{111}Ag (see Figure 11). Most of the decays of ^{111}Ag result in no γ-rays. Only 5% of the decays go to

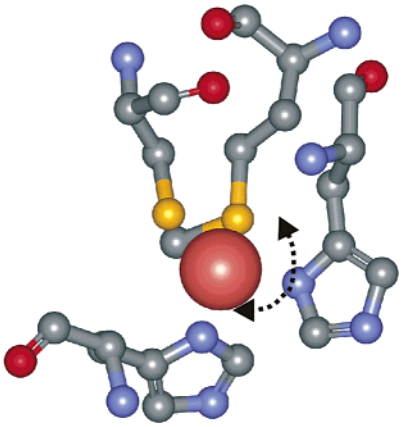

Figure 10. Structure of the metal ion binding site in spinach plastocyanin (PDB file 1AG6[48]). Probably one of the solvent-exposed histidines can take on a distribution of positions, giving rise to the unusual frequency distribution seen as a line broadening of the second and third peak in the PAC spectrum (Figure 9). For Ag, this histidine is probably in a different position, and the structure relaxes to the Cd structure on a time scale of 10 ns.[47]

the excited spin 3/2 state, and out of these, most decay to the ground state. However, 4% of these nuclei decay via the intermediate spin 5/2 state that is used for ^{111m}Cd PAC spectroscopy as well. The interpretation of the spectral change with time is that for ^{111}Ag the first γ-ray is emitted from a Cd nucleus that is still in a coordination geometry that has been adapted to Ag. That is, the 27 ps, which is the lifetime of the state from which the first γ-ray is emitted, are not enough for the structure to relax. In the time between the first and the second γ-ray (lifetime of 85 ns), the structure may relax, so that it is adapted to the Cd ion. The structural interpretation of this is that for Ag-plastocyanin one of the histidines is forming a smaller angle to the cysteine. After the decay to Cd, a larger Cys-His angle is favored, and the histidine therefore relaxes to this position. A half-life of the relaxation of approximately 10 ns was deduced from the spectra recorded at 1 °C.

4.1.1.4. Binding of Plastocyanin to Photosystem I. The biological function of plastocyanin is to accept electrons from cytochrome b/f and donate electrons to photosystem I, see Figure 13. It has been debated whether the binding of plastocyanin to its redox partner photosystem I depends on the redox state of plastocyanin, and if so, what could explain such a difference in binding? For a discussion of this, see the paper by Drepper et al.[50]

As mentioned in the Introduction to PAC spectroscopy, it is also possible to measure the rotational diffusion. Because the correlation time is proportional to the volume of the molecule, the correlation time depends strongly on whether plastocyanin is free in solution or bound to the much bigger protein complex photosystem I. The effect of different correlation times is illustrated in the previous Figure 5. In Figure 12, it is illustrated how the binding of Ag-plastocyanin to photosystem I changes the PAC spectrum by increasing the correlation time by more than a factor of 10, whereas this change is absent for Cd-plastocyanin.[47]

It is clear from Figure 12 that Ag-plastocyanin binds to PS1, whereas Cd-plastocyanin does not. In addition, careful analysis of the Ag-plastocyanin spectrum shows that the structure does not relax to the Cd-plastocyanin structure, contrary to the case of free Ag-plastocyanin. Therefore, it seems that binding of plastocyanin to photosystem I immobilizes the relaxing histidine. Thus, it must take an active part in the binding to photosystem I, and at the same time, the position that is energetically favored by the divalent ion creates a mismatch in the protein−protein interaction, possibly by breaking a hydrogen bond or creating a sterical mismatch.

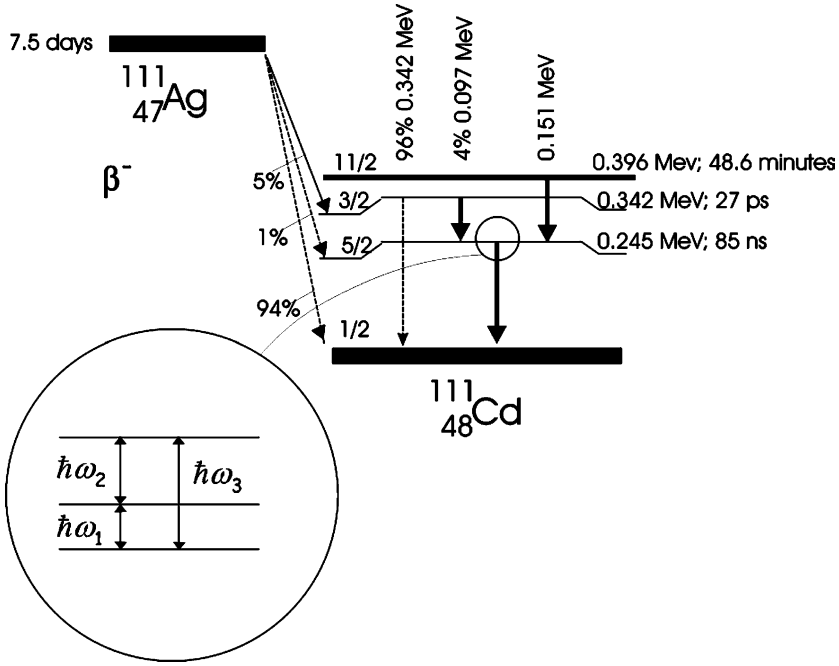

Figure 11. Schematic presentation of the decay of the two PAC isotopes ^{111}Ag and ^{111m}Cd. The arrows in boldface correspond to the γ-ray emissions detected in PAC spectroscopy for these two isotopes. Note that the intermediate nuclear level is the same for the two isotopes.

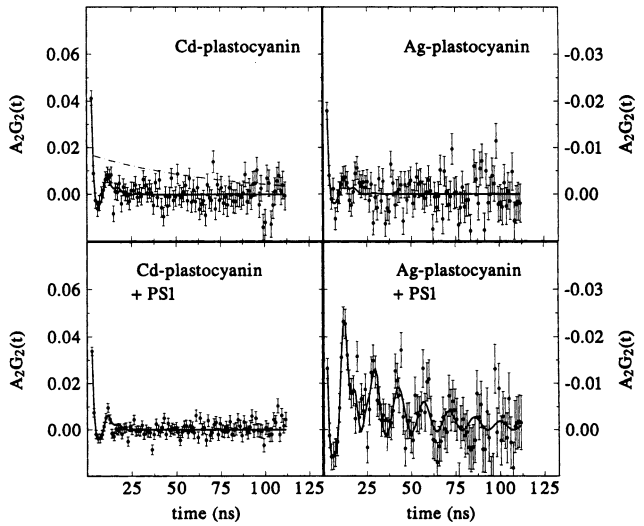

Figure 12. Binding of Cd-plastocyanin and Ag-plastocyanin from spinach to PS1. Perturbation functions of Ag- and Cd-substituted plastocyanin at 1 °C, all in the absence of sucrose, and in the absence (upper panels) and presence (lower panels) of PS1. The addition of PS1 leaves the Cd perturbation function almost unaffected, whereas it has a huge impact on the Ag perturbation function. An analysis shows that 4 ± 5% Cd-plastocyanin was bound to PS1, whereas 91 ± 11% Ag-plastocyanin was bound to PS1. The change in the spectrum for Ag-plastocyanin reflects an increased rotational correlation time, due to the binding of plastocyanin to photosystem I. Reprinted with permission from ref 47. Copyright 1999 American Chemical Society.

4.1.2. Multicopper Proteins (Laccase and Ascorbate Oxidase)

The enzymes laccase and ascorbate oxidase are members of the blue multicopper protein family, which catalyzes the oxidation of various organic substances coupled to the reduction of oxygen to water. They have four copper ions per subunit in three different sites, so-called type 1 (which is similar to the metal ion binding site in the small blue copper proteins) and type 2 and 3 sites, see Figure 14. In the case of ascorbate oxidase, X-ray diffraction revealed the structure of the different metal ion binding sites.[56] There is one mononuclear copper ion binding site per subunit in the enzyme with a cysteine, a methionine, and two histidine ligands in a distorted tetrahedral geometry. A trinuclear copper ion binding site consists of one type 2 Cu, which has two histidine ligands, and probably a water/hydroxyl ion, and an antiferromagnetically coupled type 3 Cu-pair, which is coordinated by six histidines in a trigonal prismatic coordination. In the case of laccase, X-ray diffraction data were not available before the PAC experiments. However, the similar PAC spectra suggested that the metal ion binding sites in laccase are very similar to those in ascorbate oxidase except that at the type 1 site the methionine is missing.

PAC experiments were carried out on ascorbate oxidase (*Cucurbita pepo medullosa*) and laccase (*R. vernicifera*) with Cd and Hg isotopes.[45,52−54] In the case of ^{199m}Hg, it is possible to reconstitute the enzyme fully, and the PAC spectra can be decomposed into three subspectra according to the type 1, 2, and 3 Cu sites. The assignments of the three subspectra are based on the comparison with small blue copper proteins, with type 2 depleted ascorbate oxidase spectra, and on blocking experiments with inactive mercury. Experiments with equivalent ^{199m}Hg/carrier yielded reconstitution probabilities. The experiments revealed that the type 2 site is preferentially reconstituted by Hg.[52,53]

The pure type 2 Cu site could not be reconstituted by ^{111m}Cd, probably because of the low coordination number at this site, but signals have been assigned to the type 1 and type 3 sites. At pH > 8, a single NQI was observed, which was different from the two NQIs observed at neutral pH. This NQI might originate from a Cd at the type 2 site, but Cd has at least one additional ligand, probably OH^-.[45]

The coordination chemistry for cadmium is different from that of mercury. Mercury has a tendency to form linear or almost linear complexes with sulfur ligands and the two metal ions have different ionic radii. Thus, comparing the NQIs of cadmium- and mercury-substituted metallo proteins gives information about the rigidity of the metal ion binding site. In the case of ascorbate oxidase and laccase, this comparison shows that whereas the type 1 site has a scaling factor as for the blue copper proteins indicating a high rigidity of the metal ion binding site, the type 3 site scales with a different factor, which was approximately the same for both tensor components. This site is therefore still rigid with respect to torsions but more susceptible to dilation than the type 1 site. Thus, it has been demonstrated that metal exchange properties and the relationship between the different metal ion binding sites can be followed by PAC spectroscopy.

4.2. Zinc Ion-Containing Proteins

Several hundreds of proteins containing zinc ions have been identified,[57] where the zinc ion plays a role directly in catalysis or as a structural element. The zinc ion is a closed shell d^{10} ion and is therefore invisible to most spectroscopic techniques, a fact that has led to studies of zinc ion binding proteins via substitution with other metal ions. Among these, cadmium is often an excellent probe, because it has the same charge, it is also a d^{10} closed shell ion, and most cadmium-substituted zinc enzymes are catalytically active.[58] Therefore, ^{113}Cd NMR and ^{111m}Cd PAC spectroscopy provide useful tools to monitor structure and dynamics of zinc ion-containing proteins, and this section is devoted to some illustrative examples of applications of the latter technique.

4.2.1. Metallo β-Lactamase: Dynamics at the Metal Ion Binding Sites

Metallo β-lactamases, see Figure 15, are part of bacteria's defense against antibiotics. They contain two metal ion binding sites, of which at least one must be occupied for the enzymes to function. The naturally occurring metal ion is zinc, but cadmium-substituted metallo β-lactamases are also catalytically active.[60,61]

4.2.1.1. Metal Ion Jumping between Two Sites. Both ^{111m}Cd PAC and ^{113}Cd NMR experiments have

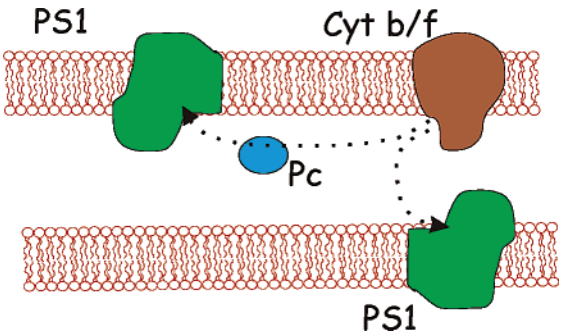

Figure 13. Function of plastocyanin in photosynthesis. Plastocyanin (Pc) plays an important role in photosynthesis-carrying electrons from cytochrome b/f (Cyt b/f) to photosystem I (PS1). The PAC experiments show that Ag-substituted plastocyanin binds much stronger to photosystem I than Cd-plastocyanin does. The results also indicate that the small difference in metal site geometries between Cd(II) and Ag(I), probably related to a shift in the position of the solvent-exposed histidine, could be involved in regulating the binding affinity as a function of redox state.

been carried out on metallo β-lactamase from *Bacillus cereus*, under conditions where one or two metal ions bind, the so-called mono- or binuclear enzyme. For the binuclear cadmium-substituted enzyme, two ^{111m}Cd PAC and two ^{113}Cd NMR signals are observed, one from each site, as expected. However, for the mononuclear enzyme, two ^{111m}Cd PAC signals but only one ^{113}Cd NMR signal are observed.[60] To understand this, it is necessary to look into the time regimes in which dynamics can be monitored by the two techniques. As described previously, dynamics can be monitored in a time regime of 0.1−100 ns by ^{111m}Cd PAC spectroscopy; see Figure 5. For ^{113}Cd NMR intermediate exchange between sites with significantly different chemical shifts will typically occur in a time regime from 0.01 to 10 ms. In the intermediate time regime of 0.1−10 μs, the system will be in slow exchange on a ^{111m}Cd PAC time scale but in fast exchange on a ^{113}Cd NMR time scale. This indicates that the ^{113}Cd NMR signal is in fast exchange, corresponding to the cadmium ion "jumping" between the two sites on a time scale of 0.1−10 μs; see Figure 16. This conclusion was supported by ^{15}N and ^{1}H NMR spectroscopy on the backbone amides and on the metal ion binding site histidines.

4.2.1.2. Dynamics of the *β*-Lactamase·*R*-Thiomandelate Complex. The design of inhibitors of metallo β-lactamases is, obviously, an important goal in the study of these enzymes. PAC spectroscopy has been applied in this context, to characterize the binding of the two enantiomers of thiomandelate to metallo β-lactamase from *B. cereus*.[62] Interpretation of the PAC spectra recorded on the β-lactamase·*R*-thiomandelate complex at −1 °C presented a considerable challenge, and no satisfactory fit was achieved with standard methods. One possible origin of this problem was dynamics occurring at the metal ion binding site. Therefore, two additional experiments were carried out, one at −20 °C and one at 30 °C. All three spectra contained one signal, which was assigned to one of the two metal ion binding sites in the enzyme. The spectrum recorded at −20 °C contained additionally two signals, which were assigned to two different coordination geometries at the other metal ion binding site; that is, the dynamical feature was "frozen out" at this lower temperature. At 30 °C, there was only one signal in addition to the signal from the first metal ion binding site. This signal was at the numerical average of the two signals found at −20 °C, as would be expected in the fast exchange regime for two equally populated species. The spectrum at −1 °C, thus, appears to be in the intermediate exchange regime, with considerable damping and broadening of the two signals found at −20 °C causing the problems with the interpretation. This is the first time such a dynamic process has been discovered and published experimentally for PAC spectroscopy applications in biochemistry. Possible structural interpretations are an on/off process of a water molecule or of the carboxylate group of the inhibitor coordinating to the metal ion. The time scale of the exchange process can be estimated to be $\tau \sim 2/(\omega_A - \omega_B) = 50$ ns at −1 °C, assuming that there is no change of sign in ω_{zz}.

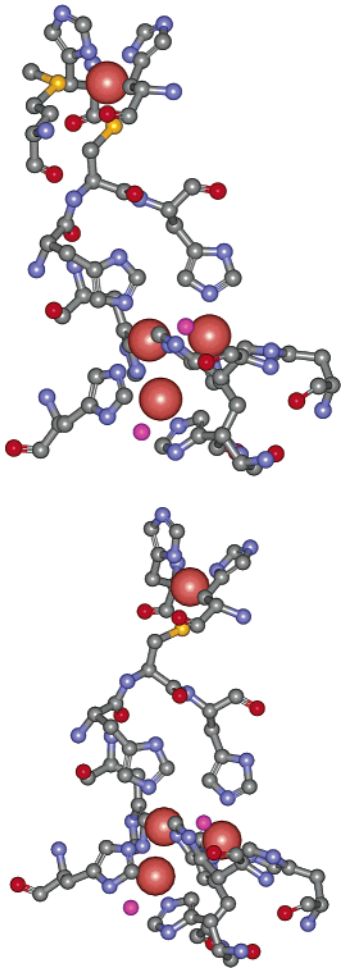

Figure 14. The enzymes laccase and ascorbate oxidase both contain four copper ions per subunit. PAC studies on *R. vernicifera* laccase showed that all copper ions can be substituted by mercury. PAC experiments with ^{199m}Hg-laccase were carried out, and signals were assigned to the different metal ion binding sites, revealing different reconstitution probabilities.[45,52−54] The upper figure shows the metal ion binding sites of ascorbate oxidase from zucchini (PDB file 1AOZ[51]). The lower figure shows the metal ion binding sites of laccase from *Trametes versicolor* (PDB file 1GYC).[55]

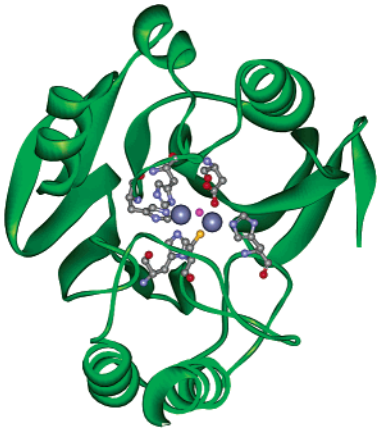

Figure 15. Metallo β-lactamases are part of bacteria's defense against antibiotics. They contain two metal ion binding sites, of which at least one must be occupied for the enzymes to function. (This figure is based on the structure of *Bacteroides fragilis*; PDB file 2BMI[59]).

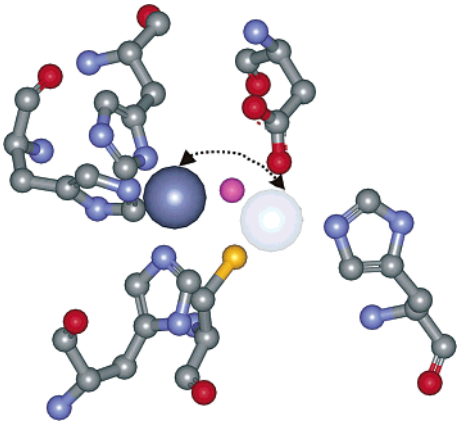

Figure 16. Dynamics at the metal ion binding sites of β-lactamase. Combined studies using ^{113}Cd NMR and ^{111m}Cd PAC spectroscopy on β-lactamase from *B. cereus* show that when only one cadmium ion is bound to the protein, this ion jumps between the two sites on a time scale between 0.1 and 10 μs.[60,61] (This figure is based on the structure of *B. fragilis*; PDB file 2BMI[59]).

A similar kind of motional narrowing has been observed for a temperature study of the M121D mutant of azurin from −196 to 95 °C, where two different NQIs are observed at low temperature and only one at high temperature (unpublished work).[63]

4.2.2. Metal Ion Binding Site Coordination Geometry of Carboxypeptidase A during Steady State Catalysis

The enzyme bovine carboxypeptidase A from pancreas reversibly cleaves/makes peptide bonds at aromatic carboxy-terminal amino acids of proteins and peptides. It binds a Zn(II) ion, which is essential to the catalytic process, with two histidine nitrogen atoms and a bidentate carboxyl group from a glutamic acid; see Figures 17 and 18. When substrate is not present, one or two water molecules also coordinate to the metal ion. Exchange of the zinc ion with Cd(II) leaves the enzyme active, and the ^{111m}Cd-substituted enzyme has been investigated during steady state conversion of the peptides Bz-Gly-Gly-L-Phe and Bz-Gly-L-Phe.[65] During the experiments, the substrate concentration was kept larger than 10 times K_M, so the dominant species in solution was

Figure 17. Carboxypeptidase A reversibly cleaves/makes peptide bonds at aromatic carboxyterminal amino acids of proteins and peptides (illustration based on the structure of bovine, pancreatic carboxypeptidase A; PDB file 1EE3[64]).

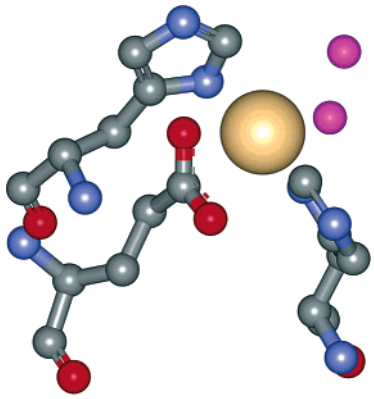

Figure 18. Metal ion binding site in carboxypeptidase A. It was possible to measure the PAC spectrum of Cd-substituted bovine, pancreatic carboxypeptidase under active conversion of substrate. On the basis of the experiments, it could be concluded that the Cd ion had to be 4- or 6-coordinated during steady state catalysis. The most probable explanation is a 6-coordinated structure with an OH^- and a carbonyl oxygen from the substrate as ligands in addition to the amino acids at the metal ion binding site[65] (PDB file 1EE3[64]).

the enzyme−substrate complex just before the rate-limiting step.

A selection of some of the Fourier-transformed ^{111m}Cd PAC spectra is shown in Figures 19 and 20. Some conclusions can be made directly by visual inspection of the Fourier-transformed spectra: If the spectrum collected in solution is compared to the spectrum obtained from a polycrystalline sample, it is clear that in the polycrystalline sample only one NQI is present, identifying itself by three sharp peaks; see Figure 19. In solution, the lines are broader. The broad lines indicate rotational diffusion and a range of similar structures and/or dynamic exchange between two or more metal ion binding site structures. In addition, at a pH above 8.3, the data can only be analyzed satisfactorily by including two different NQIs. In solution, these two NQIs have a population ratio of approximately 1:2 at pH 8.3, 9.3, and 10.5. In the crystalline state, only one conformation of the metal ion binding site is populated. In the two spectra obtained in solution under steady state conversion of Bz-Gly-Gly-L-Phe and Bz-Gly-L-Phe, only one well-defined NQI is observed and the

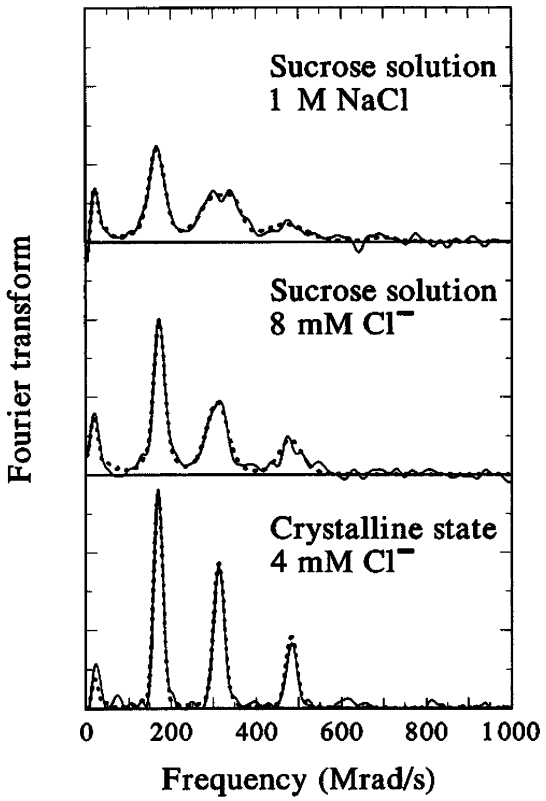

Figure 19. Fourier transform of PAC spectra in different physical states from bovine ^{111m}Cd-carboxypeptidase A at pH 7.5. The solid and dotted lines are the Fourier transforms of the theoretically fitted function and the experimental data, respectively. The crystallization results in a significant decrease in line width, because of both decreased rotational diffusion and a selection of one structural conformation. Reprinted with permission from ref 65. Copyright 1997 American Chemical Society.

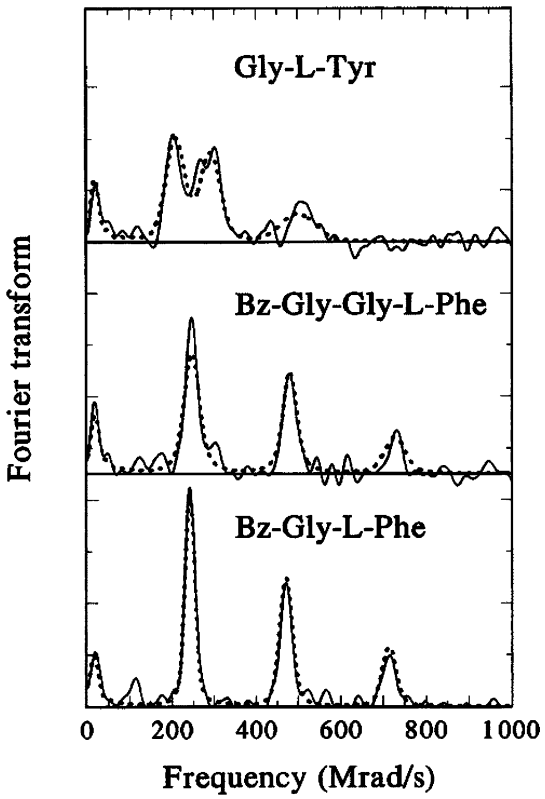

Figure 20. Fourier transform of PAC spectra of bovine ^{111m}Cd-carboxypeptidase A in the presence of the three substrates. On the basis of the spectra, it was shown by Bauer et al.[65] that the cadmium ion is not 5-coordinated during active conversion but more likely to be 6-coordinated, probably with an OH^- and a carbonyl oxygen from the substrate as ligands. Reprinted with permission from ref 65. Copyright 1997 American Chemical Society.

spectral parameters were similar for the two substrates; see Figure 20. This shows, not surprisingly, that the same mechanism is involved in the conversion of these two peptides. In contrast, the spectrum with the poor substrate Gly-L-Tyr is distinctly different from the two others, showing that the metal ion binding site coordination geometry is different in this case and that this may be the reason for the less than optimal degradation of this substrate. Spectra were also recorded with carboxypeptidase and the products (not shown); none of these resemble the spectra of the substrate complexes. This leads to the conclusion that the rate-limiting step cannot be product release.

4.2.2.1. BASIL Calculations Based on Former Crystal Structures of Carboxypeptidase. The main purpose of this study was to get information on the enzymatic process and in particular the structure of the metal ion binding site during active conversion of substrate. Therefore, BASIL calculations were carried out based on the only existing structure at that time of Cd-carboxypeptidase.[66] These showed that the NQI observed for the polycrystalline sample and the NQI dominating in solution were in accordance with the published structure, where the cadmium ion is coordinating to two histidines and a bidentate glutamic acid and one water molecule. It could be shown that the NQIs measured for the converting enzyme could not be obtained in a BASIL calculation by replacing the water molecule by any other ligand—even with large variations in the position of the replacing ligand. Thus, it could be concluded that during active conversion of substrate the cadmium ion would have to be either four-coordinated or (more likely) six-coordinated with an OH^- and a carbonyl oxygen from the substrate as ligands.

4.2.2.2. BASIL Calculations Based on a Later Crystal Structure of Carboxypeptidase. After the publication of the PAC experiments,[65] Jensen et al.[64] solved the crystal structure of Cd-carboxypeptidase under three different conditions. In all three structures, two water molecules coordinate to the metal ion. Comparing this to the NQIs measured by PAC spectroscopy suggests a simple interpretation: The two NQIs in solution above pH 8.3 are in accordance with one water molecule coordinating or two water molecules coordinating, respectively. Crystallization selects one of the two forms, but which form is selected depends on the crystallization conditions. Lowering the pH (in solution) to below 7 also selects the conformation where one water molecule is coordinating. Above pH 8.3, the two forms in solution exist in equilibrium with about 35% population of the form with two water molecules coordinating.

The comparison of the measured NQIs and BASIL-calculated NQIs based on the later crystal structure

Table 2. Comparison of BASIL Calculations Based on a Later Crystal Structure of Carboxypeptidase[64] to Experimental Values[65]

	ω_0 (Mrad/s)	η
PAC experiment		
solution	156(1)	0.29(2)
	200(2)	0.86(1) (∼35%)
powder crystal	158.4(5)	0.261(4)
active conversion of substrate (mean)	239(2)	0.15(1)
BASIL calculation		
one water molecule coordinating[66]	150	0.41
two water molecules coordinating[64a]	245−260	0.70−0.75
replacing W(401) with OH^- and W(550) with CO group[a]	262−278	0.39−0.43

[a] The latter two calculations are based on three different structures labeled 1ELL, 1ELM, and 1EE3.[64]

by Jensen et al.[64] has not been published previously. This comparison is made in Table 2 with the different structures as input for the ligand positions. The latter two calculations were based on three different Cd-carboxypeptidase structures (1ELL, 1ELM, and 1EE3). From each structure, the Cd ion in the zinc ion binding site (labeled 350) was used. As partial NQI of OH^-, a value of 349 Mrad/s was used (see appendix B).

Thus, the structure where one water molecule is coordinating[66] is a good candidate for the structure dominating in solution, whereas the structure where two water molecules coordinate[64] is a candidate for the other conformation present at high pH in solution. The latter is also a good candidate for the structure of the site under active conversion if the water molecule labeled W401 is replaced by an OH^- and water molecule labeled W550 is replaced by a carbonyl oxygen. The experimentally determined and calculated η do not compare well, because η is very sensitive to the position of the OH^-. To illustrate this sensitivity, we can use the BASIL model on the structure based on 1EE3, where the two water ligands are replaced by a carbonyl oxygen and an OH^-, respectively. For the positions in the crystal structure, the calculated ω_0 is 263 Mrad/s and η is 0.42. Moving the OH^- by 6° is enough to lower η to 0.03, whereas ω_0 is almost unchanged at a value of 264 Mrad/s. It should be stressed that we do not wish to use the BASIL model to suggest the position of the OH^- but rather to illustrate how sensitive the measured values can be to small structural changes and to stress that even if the BASIL model was perfect, it would not be possible to predict the measured NQIs better than the accuracy in the position of the ligands allows.

4.2.2.3. Comparison to Simulation of Fast Exchange of One Water Molecule. With a specific candidate for the two solution structures, it is also possible to investigate whether the line broadening observed for carboxypeptidase in solution in the absence of substrate can be ascribed to dynamic exchange between the two structures. The PAC simulator[21] can be used to investigate whether a dynamic exchange between the two structures would lead to spectra that are similar to the measured spectra; see Figure 21. Such simulations have not previously been published. As input parameters, the

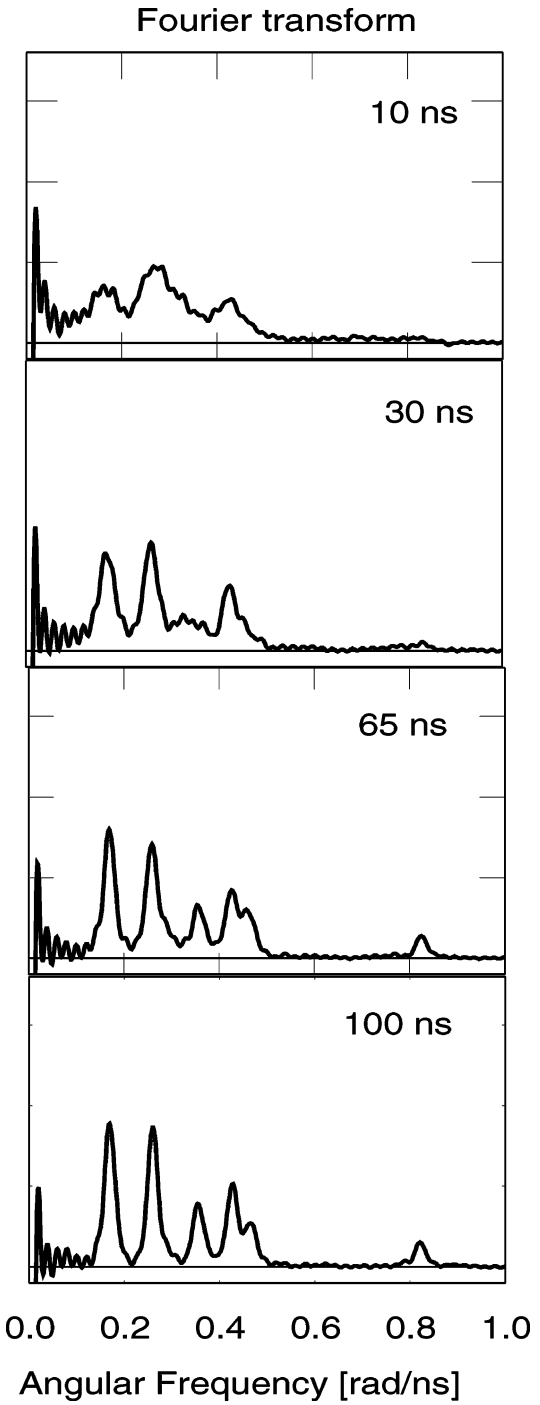

Figure 21. Simulations of PAC spectra using the PAC-simulator[21] based on dynamic exchange between two carboxypeptidase structures: one with two water molecules coordinating and one with one water molecule coordinating. The figure illustrates how the on/off process of one of the water molecules broadens the lines as the lifetime shortens. Further shortening of the lifetime will eventually lead to motional narrowing with one NQI, which will be the weighted average of the two in dynamic exchange. The lifetime of the structure with two water molecules coordinating is given in the figure. The lifetime of the structure with one water molecule coordinating was chosen to be twice as long, giving a population ratio of 1:2 as in the experimental PAC observations. A lifetime of 30 ns of the structure with two water molecules coordinating gives good agreement with the experimental data.

magnitude and the orientation of the NQI were calculated in a BASIL calculation based on the structure around the cadmium ion binding site (labeled 350) in the structure published as 1EE3.[64] The dynamic water was assumed to be the water molecule labeled HOH550. The results suggest that the line broadening found in the carboxypeptidase spectra is due to dynamic exchange of this coordinating water molecule on a time scale of the order of 30 ns. This is in the same order of magnitude as what is observed for β-lactamase in the presence of *R*-thiomandelate (see above) and for water coordinating to calcium in calbindin, where it has been observed that the residence time of the two water molecules is in the range of 5 ns to 7 μs, much longer than for calcium-coordinated water in solution.[67]

4.2.3. Structure of the Metal Ion Binding Site in Carbonic Anhydrase

Carbonic anhydrase is a zinc enzyme that catalyzes the reaction $H_2O + CO_2 \leftrightarrow H^+ + HCO_3^-$ and the hydrolysis of various esters. It contains one zinc ion per molecule, which is essential for the catalytic activity. It is known from X-ray diffraction data that the Zn(II) ion is surrounded by three histidine residues and a solvent ligand in a slightly distorted tetrahedral geometry, see figure 22.[72,73] The catalytically important Zn(II) can be substituted by other divalent ions, but only Co(II), Cd(II), and Mn(II) enzymes remain catalytically active.[69,74,75] The activity of the Zn(II) enzyme depends on the pH with a p*K* of 7.3, whereas at this pH, the Cd(II) enzyme is inactive because the p*K* for the Cd(II) enzyme is shifted to 9.1. For both enzymes, this indicates that the hydrolysis of CO_2 and the various esters requires the ionization of a group for which the pK_a depends on which metal ion is present in the protein.[9,23,76] The pH range where the Cd(II) enzyme is active is shifted toward to higher pH as compared to the native enzyme, probably because the pK_a of the titrating group is dependent on the ionic radius of the metal ion.

The PAC spectra of the human Cd(II) enzyme showed a pH dependency[69] where the spectra changed significantly between pH 8 and pH 10. This change in the NQI is in correlation with the pH profile of the measured hydrolytic activity for the Cd(II) enzyme. It was suggested that the ionization of the metal-dependent group is the transformation of a metal-ligated water molecule to a hydroxyl ion ligand, and this coordinated hydroxyl group is assumed to attack the CO_2 molecule and convert it to HCO_3^-. BASIL calculations carried out using the crystal structure as input provided satisfactory results as compared to the experimental data, assuming that the metal-bound solvent ligand is H_2O at low pH and OH^- at high pH.[70]

The effect of different inhibitors of the native enzyme was investigated by PAC spectroscopy. Several anions (iodide, bicarbonate, and chloride) inhibit the enzyme. These inhibitors do not change the PAC spectra drastically. The small influence of Cl^- binding at low pH can be explained by the nearly equal partial NQI for water and Cl^-.

Imidazole is a competitive inhibitor of carbonic anhydrase.[77] Addition of imidazole changed the PAC spectra both at low and at high pH.[71] The measured NQI indicates that the metal binding site for this inhibitor is different from the activity-linked ionization site, which implies that the metal becomes five-coordinated in the presence of the imidazole molecule. Because of the fact that the inhibition kinetics is almost the same in the case of the native and the Cd(II) enzyme, it is suggested that the imidazole coordinates as a fifth ligand to the zinc in the native enzyme as well.[70] Because imidazole competes with CO_2 for binding to the enzyme, it is suggested that the imidazole binding site is close to that of CO_2 in the enzyme.

All of the PAC spectra of carbonic anhydrase were recorded on samples with the Cd(II) enzyme in 40−60% w/w sucrose or in a frozen state to avoid the problems arising from the rotational diffusion. Measurements were carried out under several conditions such as without sucrose at −196 °C and with 50% w/w sucrose at 22 °C. Under both conditions, the spectra appeared to be much damped. The spectra could be fitted with about 15% distribution in the NQI frequencies. This indicates that the ligand geometry is very flexible changing from molecule to molecule.

4.2.4. Alcohol Dehydrogenase

The enzyme alcohol dehydrogenase from horse liver (LADH) catalyzes the reversible oxidation of primary and secondary alcohols using NAD^+ as a coenzyme. A Zn(II) ion essential for the catalytic process is bound to the protein by two cysteine sulfur atoms and one histidine nitrogen atom. When substrate is not present, a water molecule is the fourth metal ion ligand, see Figure 23. The cadmium ion-containing enzyme is still active, although not as active as the native zinc ion-containing enzyme. A large number of complexes of LADH with coenzyme and inhibitors or substrates have been studied by PAC spectroscopy; see references in Table 3.

4.2.4.1. pK_a of Metal Bound Water. For the zinc ion-containing enzyme, a group affecting the association rate of both NAD^+ and NADH has a pK_a of 9.6.[79] Kvassman and Pettersson interpreted this as ionizatin of the metal ion bound water molecule.

LADH with the Zn(II) ion replaced by ^{111m}Cd(II) has been investigated by PAC spectroscopy for a series of pH values, to study whether a titrating group would also be found after replacement of the metal ion and whether this would affect the pK_a.[18] For Cd(II), the pK_a is expected to shift upward, because the ionic radius of Cd(II) is larger than the ionic radius of Zn(II). The Fourier-transformed spectra for the different pH values are shown in Figure 24. The three peaks expected in the Fourier transform for a ^{111m}Cd PAC experiment are not resolved here. For example, at pH 7.9, basically only one broad peak is found at 450 Mrad/s. This is because two peaks have coalesced into one, and the third, which should be found at 900 Mrad/s, is buried in the noise. A change occurs from a low pH form, with a peak at 450 Mrad/s, to a high pH form, with a peak at 250

Table 3. Applications of PAC Spectroscopy in Biochemistry and Biology[a]

proteins	isotope	native ion	scientific issue	coordinating ligands[a]	refs
			zinc ion-containing proteins		
human carbonic anhydrase B and C	^{111m}Cd	Zn	structure of metal ion binding site; two different coordination geometries (low and high pH) enzymatic mechanism (CO_2 binds to Cd(II) in a pentacoordinate structure)	low pH: 3His, H_2O high pH: 3His, H_2O, OH^-	69−71, 117, 122, 123
bovine carboxypeptidase A	^{111m}Cd	Zn	structure of metal ion binding site (resting state vs active converting enzyme), rigidity/flexibility of metal ion binding site	2His, bidentate Glu, solvent molecule/substrate	65, 117, 124, 125
yeast and bovine superoxide dismutase	^{111m}Cd	Cu, Zn	structure of metal ion binding site, enzymatic mechanism rotational diffusion—development of data analysis	4His 3His, 1Asp	10, 20, 117, 119, 126, 127
horse liver alcohol dehydrognase	^{111m}Cd	Zn	enzymatic mechanism structure of metal ion binding site [enzyme, binary complex (+ coenzyme), ternary complex (+ coenzyme + inhibitor/substrate)], open + closed conformations flexibility/rigidity of the metal ion binding site structural change (pH dependency), binary complex with NADH: two coordination geometries (rigid)	catalytic: 1His, 2Cys, H_2O/OH^- structural: 4Cys	18, 20, 37, 54, 61, 65, 111, 117, 125, 128, 129
angiotensin converting enzyme from rabbit lungs	^{111m}Cd	Zn	metal binding, coordinating ligands	modeled by 2His, 1Cys, solvent	130
β-lactamase (*B. cereus* and *Aeromonas hydrophilia*)	^{111m}Cd	2Zn	structure and interaction of metal ion binding sites dynamics of metal ion binding site on a 0.1−10 μs time scale combination of PAC and NMR spectroscopy metal ion binding to β-lactamase and geometry of metal ion binding sites difference in binding between two entatiomers of thiomandelate combination of PAC and EXAFS spectroscopy	3His, OH^- (bridging), Asp, Cys, His, H_2O, OH^- (bridging)	60−62, 131, 164
2Zn-insulin	^{62}Zn	Zn	feasibility of biological ^{62}Zn PAC spectroscopy	6His	132
metallothionein from rabbit liver	^{199m}Hg ^{111m}Cd	Zn, Cu, Cd, Hg	coordination geometry of mercury and cadmium in metallothionein	2- or 4Cys	133, 134
			copper ion-containing proteins		
yeast and bovine superoxide dismutase	^{111m}Cd	Cu, Zn	structure of metal ion binding site, enzymatic mechanism rotational diffusion—development of data analysis	4His, 3His, 1Asp	10, 20, 117, 119, 126, 127
laccase (*R. vernicifera*)	^{111m}Cd ^{199m}Hg	4 Cu (type-123)	coordination geometry of metal ion binding site (function) NQI for methionine different coordination for cadmium and mercury metal reconstitution of the three types of sites depends on the type of metal ion (Cd/Hg) interaction between the different metal ion binding sites	type-1: Cys, 2His type-2: 2His, H_2O anti-ferromagnetically coupled Cu pair (type-3): 6His	45, 52, 53
ascorbate oxidase (*C. pepo medullosa*)	^{111m}Cd ^{199m}Hg	4 Cu (type-123)	coordination geometry of metal ion binding site (function) NQI for methionine different coordination for Cd and Hg Hg derivatives to block and deplete the Cu sites	type-1: 2His, Met, Cys type-2: 2His, $1H_2O$ anti-ferromagnetically coupled Cu pair (type-3): 6His	45, 52−54
azurin (*P. aeruginosa* and *A. denitrificans*), H117G-azurin, H117G-azurin + imidazole derivatives, Met121 mutants of azurin	^{111m}Cd ^{111}Ag ^{199m}Hg	Cu	structure of metal ion binding site, role of methionine, effect of exogenous ligands as opposed to amino acids from the protein, substitution of methionine to histidine, relaxation of structure after radio nuclear change from monovalent to divalent metal ion adsorption of azurin on a flat surface	2His, 1Cys His,Cys, solvent other	27, 33, 45, 46, 53, 63, 110, 112, 125, 135

Table 3 (Continued)

proteins	isotope	native ion	scientific issue	coordinating ligands[a]	refs
			copper ion-containing proteins		
azurin, Met121Asn azurin (*P. aeruginosa*)	^{111m}Cd	Cu	development of a criteria of distinguishing between one and two NQIs	2His, Cys, (Asn + solvent?)	129
plastocyanin (*spinacea*) Leu12Ala, Leu12Asn, and Leu12Glu plastocyanin	^{111m}Cd ^{111}Ag ^{199m}Hg	Cu	structure of metal ion binding site and binding of plastocyanin to photosystem I as a function of redox state metal ion binding site flexibility adsorption of plastocyanin on a flat surface	2His, 1Cys	45, 47, 49, 110
stellacyanin (*R. vernicifera*)	^{111m}Cd ^{199m}Hg	Cu	structure of metal ion binding site adsorption of stellacyanin on a flat surface	2His, 1Cys, Gln	27, 45, 53, 110
hemocyanin (*Carcinus aestuarii*)	^{111}Ag	Cu	interaction between and coordination geometry of two metal ion binding sites	3His, water	136
hemocyanin (*Eurypelma californicum)*	^{199m}Hg	Cu	binding of Hg to the binuclear metal ion binding site effect of Hg on metal ion binding site geometry		137
bleomycin	^{111}In	Fe, Co, Cu, In	In-bleomycin complex and In-bleomycin binding to DNA interpretation difficult due to after effects	not stated	138
			iron, mercury, or molybdenum ion-containing proteins		
metallo porphyrin (synthetic) phthalocyanine (synthetic)	^{111}In	(Fe)	EFGs of porphyrins and phthalocyanine dynamics in organic solvents phthalocyanine gives much sharper peaks than porphyrins	porphyrins/ phthalocyanine + Cl^-	139
human serum transferrin	^{111}In	Fe	TIPAC as a tool for distinguishing healthy serum from cancer serum the difference between healthy and cancer serum does not seem statistically significant	unspecifically bound or Fe-metal ion binding sites	140
human and rat serum transferrin	^{181}Hf	Fe	in vivo and in vitro hafnium binding to serum transferrin binding of hafnium to two different binding sites relaxation of metal ion binding site structure comparison of human and rat serum transferrins	not stated likely Fe ligands	82, 85, 87−89
human serum transferrin	^{111}In	Fe	In-binding to transferrin motivated by clinical use of In, exchange of In between transferrin and metal chelators tropolone and acetyl-acetone poor resolution due to after effects of EC of In	not stated likely Fe ligands	141
ovotransferrin	^{181}Hf	Fe	internal protein dynamics and the hydrodynamic volume do the two different observed NQIs represent different sites or both sites under different conditions	not stated likely Fe ligands	83−86
human and bovine lactoferrin	^{181}Hf	Fe	comparison of lactoferrin and other transferrins	not stated likely Fe ligands	90
rubredoxin (*Desulfovibrio gigas*)	^{199m}Hg	Fe	structure of metal ion binding site in Hg-substituted rubredoxin	4Cys	142, 143
FeMo cofactor in nitrogenase, and molybdenum storage protein	^{99}Mo	Mo	in vivo and in vitro identification of Fe−Mo-cofactor in nitrogenase and molybdenum storage protein in *A. vinelandii, K. pneumonia,* and *R. capsulatus*	1Mo:3Fe:3S cluster	106−109
mercury reductase (MerA) and MerR	^{199m}Hg	Hg	coordination geometry at the metal ion binding site	2 Cys (MerA) 3Cys (MerR)	92
			peptides and proteins not containing metal ions, DNA, liposomes, etc.		
bovine serum albumin	^{152}Eu ^{133}Ba ^{147}Nd ^{160}Tb	none	effect of different chemical forms on sum-peak, TIPAC	unspecifically bound	42, 144−146
bovine serum albumin	^{111}In	none	molecular dynamics and conformational changes	unspecifically bound	147

Table 3 (Continued)

proteins	isotope	native ion	scientific issue	coordinating ligands[a]	refs
peptides and proteins not containing metal ions, DNA, liposomes, etc.					
bovine serum albumin	^{111}In, ^{111m}Cd	none	rotational diffusion, backbone fluctuations, effect of hydrostatic pressure on rotational correlation, development of methodology	EDTA or DTPA-labeled	34, 148, 149
oligopeptides	^{199m}Hg	none	Hg coordination of oligopeptides containing cysteine, histidine, and tyrosine	cysteines, histidines, or tyrosines	150, 151
polyglutamic acid	^{111}In	none	helix−random coil conformational transition		152
bovine trypsinogen	^{199m}Hg	none	internal dynamics in trypsinogen; immobilization by pancreatic trypsin inhibitor	2Cys	153
DTPA-labeled peptides: oxytocin; cholecystokinin; Gly-Trp; ristocetin	^{111}In ^{111m}Cd	none	studies of dynamics of peptides/proteins	DTPA-labeled	34, 154
bovine pancreatic ribonuclease A	^{111}In	none	rotational correlation	reduced disulfide bridge	101
mice unspecific	^{111}In	none	in vivo studies on mice (time-integrated PAC)	EDTA, NTA, citrate, and Cl_3^-	101
liposomes	^{111}In	none	dynamics of DTPA-labeled membranes	DTPA-labeled	104, 105, 155−157
liposomes	^{111}In	none	in vivo degradation of liposomes in liver and spleen	complexed with nitrilotriacetic acid	104, 105
liposomes	^{111}In	none	following the digestion of the liposomes by phospholipase	DTPA-labeled	156
liposomes	^{111}In	none	following the in vivo digestion of the liposomes in mice	nitrilotriacetic acid	102, 103
liposomes	^{111}In	none	reviews describing the use of PAC spectroscopy for developing liposomal drugs	nitrilotriacetic acid and other	99, 100
calf thymus DNA	^{111m}Cd ^{111}In	none	binding of cadmium and indium to DNA, radiation damage measurements of correlation times	unspecifically bound	94, 95, 100, 158−161
calf thymus DNA	^{111m}Cd ^{111}In	none	changes in DNA flexibility after irradiation with γ-rays and neutrons	unspecifically bound	96−98
designed TRI α-helical peptides	^{111m}Cd	none	coordination geometry of cadmium in peptides designed to bind metal ions	3Cys and possibly 3Cys, H_2O	162
penicillamine	^{199}Hg	none	binding of mercury to penicillamine	Hg(II) occurs in 2−4-fold coordination	163

[a] In some of the listed studies, extraneous ligands replace a metal bound water molecule; these extraneous ligands are not listed for all studies.

Mrad/s. This fits nicely with a single pK_a of 11.0. The fact that the change with pH is detected with PAC spectroscopy demonstrates that the titrating group must be positioned very close to the metal ion. In addition, the pK_a is shifted upward by 1.4 unit, strongly indicating that it is indeed ionization of the metal bound water molecule. The small peak at about 90 Mrad/s is due to migration of a small fraction of the radioactive cadmium into the so-called structural metal ion binding site of the enzyme. In addition, pH titrations were performed from pH 8 to 11.5 for the LADH·NAD^+ and LADH·NADH complexes. With NAD^+ bound to the enzyme, the pK_a of the metal ion bound water molecule is lowered to 9.6, probably due to the positive charge on the coenzyme. With NADH, no pK_a was found, probably because it is outside the tested pH range. Kvassman and Pettersson[79] found that a group with a pK_a of 7.6 affects the dissociation rate of NAD^+ from the enzyme and that a group with a pK_a 11.2 affects the dissociation rate of NADH from the enzyme, in good agreement with the PAC data, assuming an upward shift of the pK_a for the cadmium-containing enzyme.

4.2.4.2. Two Coordination Geometries for the LADH·NADH Complex but Only One for the LADH·NADH·DMSO Complex. The spectrum recorded for the LADH·NADH complex turned out to have an interesting feature; see Figure 25. From the theory of PAC spectroscopy, it is known that a given coordination geometry in general gives rise to three peaks in the Fourier transform of the perturbation function for ^{111m}Cd and that the amplitude of the first peak is larger than (or equal to) the amplitude of the second peak. However, the experimental data seemed

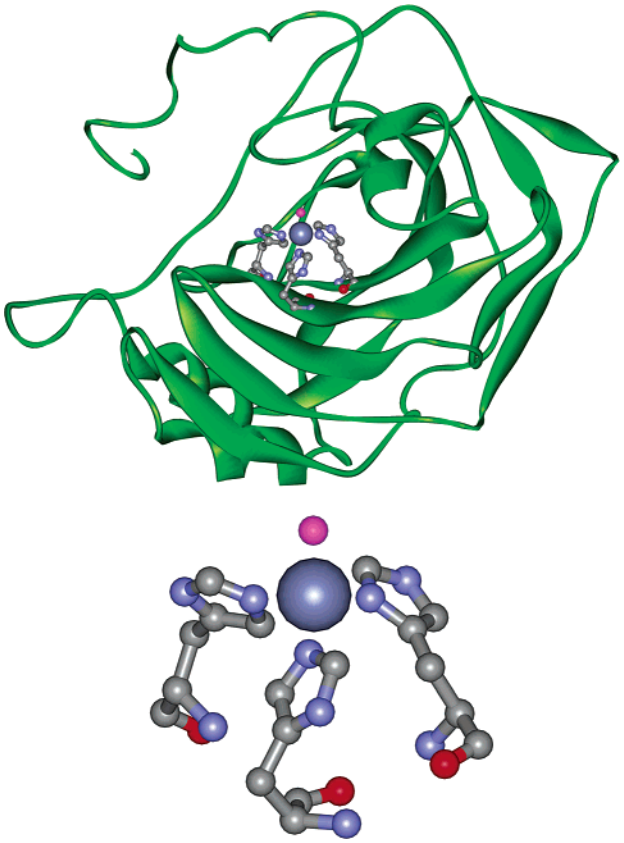

Figure 22. Human carbonic anhydrase. PAC studies on this enzyme have been carried out at several pH values and complexed with different inhibitors.[9,69−71] It has been shown that at low pH the fourth ligand is a water molecule, whereas at high pH the fourth ligand is a hydroxyl group. Imidazole acts as an inhibitor, and coordinates as the fifth ligand to the zinc ion (PDB file 1CA2[68]).

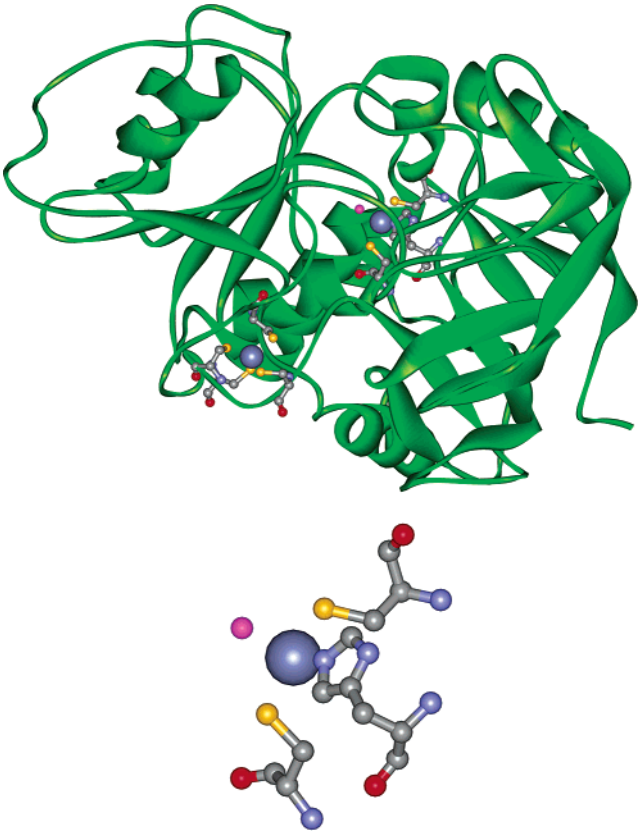

Figure 23. Structure and active metal ion binding site coordination geometry for the enzyme horse LADH. Several PAC studies of alcohol dehydrogenase have been carried out; see Table 3. Examples presented in the text are the determination of the pK_a of the metal ion bound water molecule and the puzzling discovery that two different metal ion coordination geometries exist for the enzyme in the complex with the coenzyme NADH[18] (PDB file 1JU9[78]).

to show the opposite, i.e., the first peak at about 450 Mrad/s has the lowest amplitude. The only reasonable explanation is that two coordination geometries are present and that the largest peak is actually the sum of two peaks, which accidentally coincide. This is further supported by the presence of two small peaks at a higher frequency (about 1150 Mrad/s), which are the third peaks for the two signals, respectively. The structural origin of the two signals was at the time a puzzle that was not solved. Recently, this problem was solved by a high resolution (1 Å) crystal structure of the LADH in complex with NADH.[80] It was found that the metal ion bound water molecule may occupy two different positions, one of which is probably related to the activation of the coenzyme for hydride transfer.

Adding DMSO to the solution clearly changed the spectrum, see Figure 25, showing that a ternary complex had formed. Furthermore, only one signal was found, and it is very similar to one of the two signals from the binary LADH·NADH complex. This indicates that DMSO stabilizes one of the two forms, and the exceptionally sharp lines indicate that it is a very rigid structure.

4.3. Other Applications

4.3.1. Internal Dynamics of Transferrin

One of the most extensive PAC studies in biology is the one carried out on hafnium bound to transferrins (human and bovine lactoferrin, ovotransferrin, and human and rat serum transferrins[82−90]). Transferrins are iron transporting proteins, and one reason that hafnium binding to transferrins is interesting is that it is assumed to be transported in the same way as plutonium. The protein structure and the metal ion binding site coordination geometry are shown in Figure 26. By ^{181}Hf PAC experiments, it has been possible to follow the population of two different metal binding sites—one in the N-terminal lobe and one in the C-terminal lobe. One dominates at low pH and the other at high pH. The distribution further depends on salt and hafnium concentrations, temperature, and incubation time.[89] The two metal ion binding sites must experience the same overall tumbling of the molecule; therefore, any difference in the fitted rotational correlation time must be attributed to differences in the internal dynamics of the protein in the regions of the two sites. This was studied in detail for ovotransferrin by Schwab et al.[84] By plotting the relaxation constant, λ, as a function of T/ξ, where T is the temperature and ξ is the viscosity of the sample, it was possible to separate the internal dynamics from the rotational diffusion. The functionality that was assumed was $\lambda = \lambda_0 + A\,T/\xi$. The intercept, λ_0, was interpreted as internal dynamics and was found to be significant and of the order of 30−40 MHz.

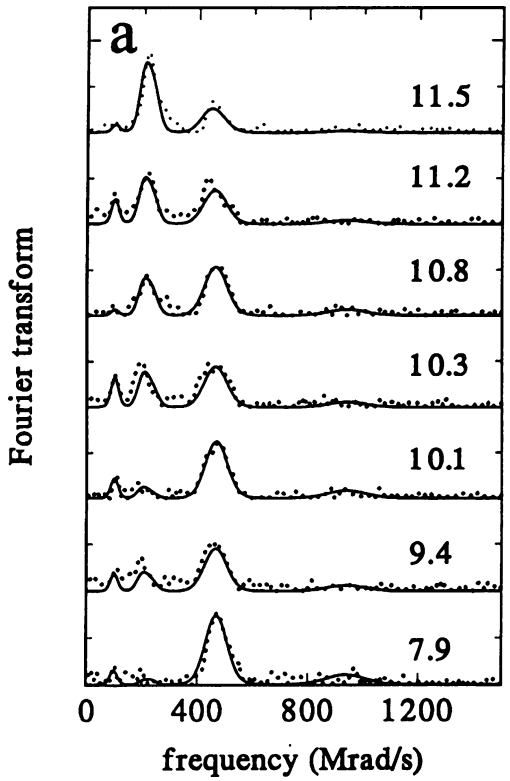

Figure 24. Fourier transformations of the perturbation functions of Cd-LADH as a function of pH. Dots, experimental data; full line, fit. The spectral changes as a function of pH fit a single pK_a of 11.0, probably originating from the metal bound water molecule.[18] Reprinted with permission from ref 18. Copyright 1995 American Chemical Society.

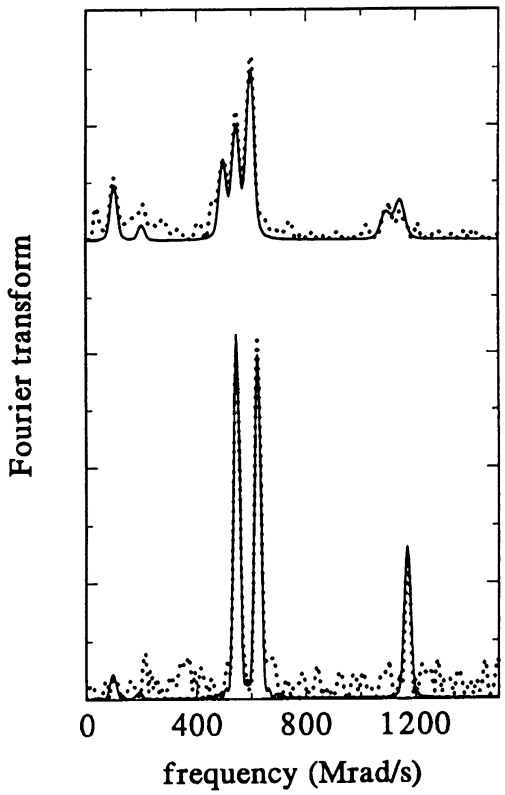

Figure 25. Binding of coenzyme and an inhibitor to horse LADH. Fourier transformation of ^{111m}Cd the perturbation functions from the binary complex between LADH and NADH (upper panel) and the ternary complex with LADH, NADH, and DMSO (lower panel).[18] Dots, experimental data; full line, fit. For the LADH·NADH complex, two different coordination geometries give rise to two NQIs, indicated by the fact that more than three peaks appear in the spectrum. Adding DMSO, a single very well-defined metal ion binding site coordination geometry is found, perhaps the most beautiful PAC spectrum recorded for a biological sample. Reprinted with permission from ref 18. Copyright 1995 American Chemical Society.

4.3.2. Enzymatic Heavy Metal Detoxification

A bacterial enzyme, so-called mercury reductase or MerA, catalyzes the conversion of Hg^{2+} into nontoxic Hg.[91] The expression of the MerA enzyme is regulated by another mercury binding protein, MerR, repressing the expression of MerA when Hg^{2+} is not present or present at only very low, below 10 nM, concentrations. A number of ^{199m}Hg PAC studies have been carried out on small model systems and on the MerR and MerA proteins, to determine the coordination geometry at the metal ion binding site.[92] The spectral characteristics of a measurement on the MerR protein were compared to spectral characteristics of two-, three-, and four-coordinate model complexes, and a striking resemblance was found with a trigonal model complex with sulfur ligands, see Figure 27. Similarly, a ^{199m}Hg PAC study of the MerA enzyme was carried out in an investigation providing a starting point for an understanding of the catalytic function of the enzyme. This showed that when the enzyme is incubated with $Hg(CN)_2$ and radioactive mercury, two different coordination geometries coexist in solution. The interpretation is that one represents Hg^{2+} bound by two cysteine amino acids of the enzyme, whereas the other represents $Hg(CN)_2$.

This study is unique in the sense that the native proteins actually function with mercury, and consequently, it is not necessary to exchange the naturally occurring metal ion with another element in order to perform PAC experiments. In addition, the study provides fundamental understanding of heavy metal detoxification, which in combination with other experimental and theoretical data constitutes the basis for development of heavy metal detoxification technologies.

4.3.3. Structure and Dynamics of DNA

The binding of metal ions to DNA is interesting, both in order to understand the effect of metal ions on the conformation of DNA and as a tool for studying changes of DNA caused by other effects such as ionizing radiation. The first to apply PAC spectroscopy to studies of DNA were Vis et al.,[94] who used ^{111m}Cd PAC to study the influence of temperature on the binding of cadmium to DNA. This study was mostly carried out with TIPAC. It was found that at 80 °C, the time-integrated anisotropy was lower than that observed at 23 °C, indicating a more rigid binding of cadmium to DNA at 80 °C, probably at the inner side of the unwound DNA. Because only the TIPAC was measured, the decrease in anisotropy could also reflect a higher fraction of bound cadmium to unbound cadmium at 80 °C.

Kalfas et al. studied the binding of indium to single- and double-stranded calf thymus DNA by time

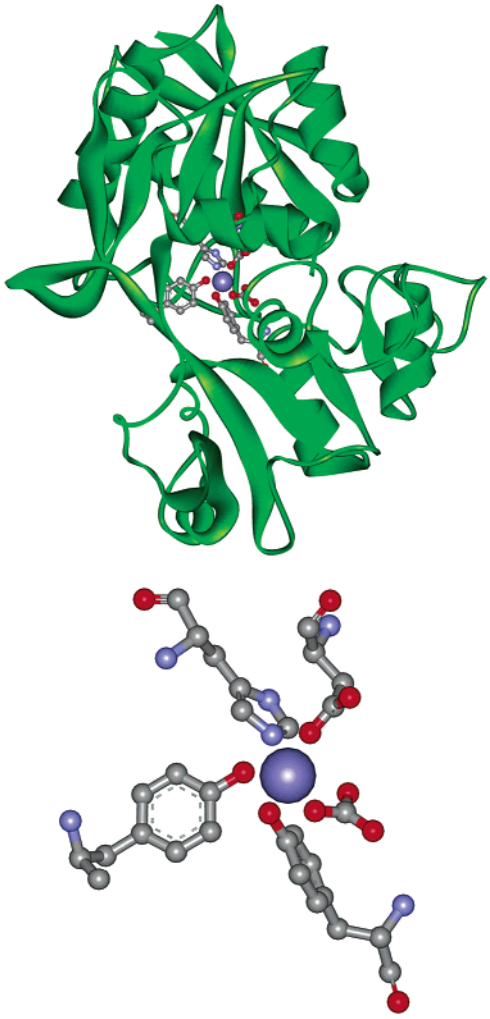

Figure 26. Structure and metal ion binding site coordination geometry of the N-terminal lobe of human serum transferrin. This metal transporting protein has been studied in detail by ^{181}Hf PAC (PDB file 1D3K[81]).

differential ^{111}In PAC spectroscopy.[95] The data show a significant difference, which was interpreted as an increase of the correlation time from 62 ± 10 ns for single-stranded DNA to 82 (+5 −4) ns for double-stranded DNA, indicating a higher rigidity of double-stranded DNA. At the time of this publication, no method for analyzing data with correlation times in the intermediate regime had been developed. Therefore, in the data analysis, the effect of the rotational correlation was assumed to be an exponential damping of the static correlation function. This analysis led to very broad frequency distributions of the order of 40−50%. However, the product of the correlation time and the smallest angular frequency is in this case in the order of 0.5, which is in the intermediate regime. It is therefore likely that methods developed later for analysis in the intermediate regime[20] could affect the interpretation of these data and allow for an analysis with less frequency distribution. Despite this, and the potential problems with after effects from the EC of ^{111}In to ^{111}Cd, the paper was the first important step in using ^{111}In PAC as a tool for studying dynamics of DNA, and the conclusions will probably remain unaltered. Further studies of indium bound to DNA are listed in Table 3.

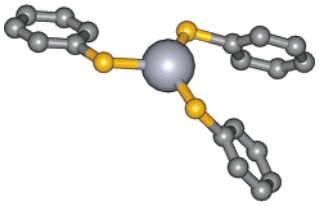

Figure 27. Structure of a trigonal planar mercury complex with three sulfur ligands. ^{199m}Hg PAC spectra of this compound are very similar to ^{199m}Hg PAC spectra of the MerR protein involved in heavy metal detoxification in bacteria. Thus, it is believed that a similar coordination geometry is found in the enzyme.[92,93]

These investigations constituted and made the basis for later ^{111}In PAC studies of the effect of ionizing radiation on DNA.[96−98] In these studies, ^{111}In is added to DNA irradiated by neutrons or γ-rays. An example is shown in Figure 28 from ref 97. The data show an increased rigidity of the DNA at doses of 1 Gy as observed by an increase of the correlation time of the fraction of the perturbation function attributed to DNA-bound indium (other fractions are free indium, indium aggregates, and indium bound to glass surfaces, etc.). At doses higher than 2−5 Gy, the correlation time starts to decrease again. This is illustrated in Figure 29 from ref 98, where the correlation time is shown as a function of dose for different salt concentrations and for irradiation of DNA with γ-rays and neutrons, respectively. This dependence on the radiation dose is explained in the following way: At the doses giving maximal correlation times, the torsional and/or rotational mobility decreases because the bonding between successive near base pairs held by the DNA stacking forces is disrupted, leading to a "less tight" formation and therefore slower rotational diffusion.[98] An alternative explanation could possibly be that the breaking of bonding between successive near base pairs could create sites that bind indium stronger. At higher doses, the irradiation causes lesions creating smaller segments with smaller correlation times. The data also show that the neutrons are about 35 times more effective, i.e., give maximal rotational correlation times at 35 times smaller doses than the ^{60}Co γ-rays. These studies provide information on the structural and dynamic properties of DNA lesions that may have implications for our understanding of radiation damage in living organisms.

4.3.4. In Vivo Studies

The advantages of PAC spectroscopy for in vivo studies are that it is noninvasive, no external fields or similar perturbation of the system is necessary, and highly specific information about the immediate surroundings of the PAC isotope is obtained. The tricky part, of course, is to get the PAC isotope into selected parts of an organism, for example, proteins or cellular compartments.

4.3.4.1. Use of PAC Spectroscopy in Liposomal Drug Research. Important published biological applications of PAC spectroscopy in biological systems are the development of liposomal drug treatments and diagnosis of cancer, as well as treatment of fungal infections. These applications have been

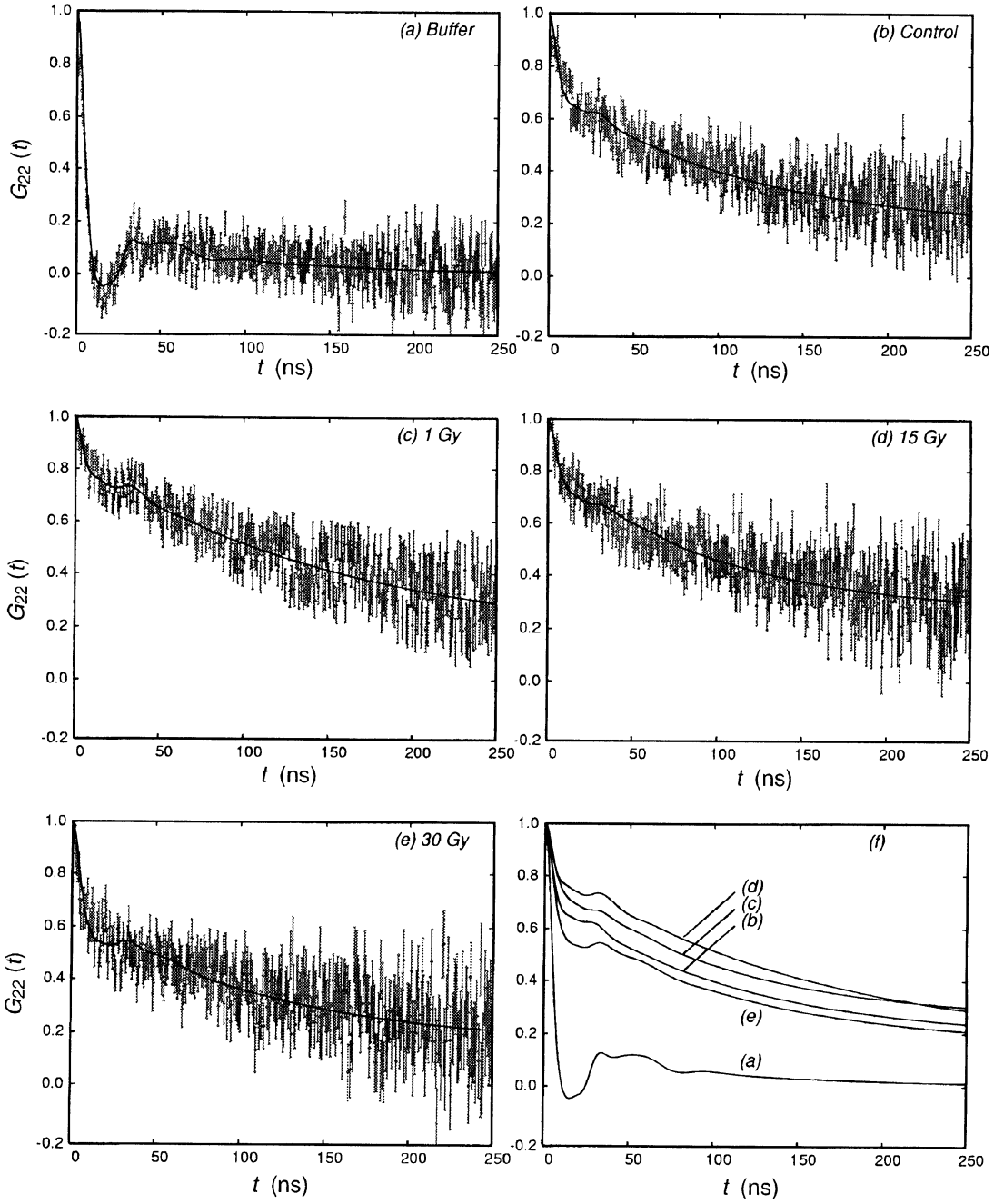

Figure 28. ^{111}In PAC experiments on calf thymus DNA exposed to different doses of ionizing radiation.^{111}In in buffer (a), ^{111}In added to nonirradiated DNA (b), and ^{111}In added to DNA irradiated with 1 (c), 15 (d), and 30 (e) Gy. (f) The theoretical fits are superimposed. The rotational correlation time increases for DNA exposed to 1 Gy, indicating an increased rigidity of the structure around indium at this dose. Reprinted with permission from ref 97. Copyright 2001 Radiation Research.

reviewed by Forssen[99] and by Baldeschwieler and Schmidt.[100] To show the diversity of applications of the technique, we have selected a few of the pioneering works using TIPAC. For a more complete survey of the subject, the reader is referred to the two reviews.[99,100]

4.3.4.1.1. In Vivo Studies on Mice. Meares and Westmoreland[101] have carried out TIPAC on living mice; see Figure 30. The purpose of this study was to show the applicability of PAC on living animals as a potential powerful tool for studying the in vivo fate of macromolecules. Four different compounds were studied as follows: ^{111}In(III) bound to EDTA, citrate, chloride, and nitrilotriacetate. Of these, the EDTA complex with ^{111}In(III) was extremely stable as judged from a distinctly higher value of $\bar{G}_{22}$ and the fast excretion in the urine. The other three complexes showed uniformly low values of $\bar{G}_{22}$ of about 0.4 indicating that the indium ions are displaced from these ligands and bind to proteins in the body.

Later, Hwang and Mauk used TIPAC on living mice to follow the in vivo degradation of lipid vesicles.[102] The ^{111}In(III) was bound to the weak chelator nitrilotriacetic acid. This complex was encapsulated in lipid vesicles and injected in mice. Upon alteration of the membrane, the ^{111}In(III) was released from the liposomes and became bound to macromolecules. This change could be observed as a decrease of $\bar{G}_{22}$ from 0.68 for indium bound to

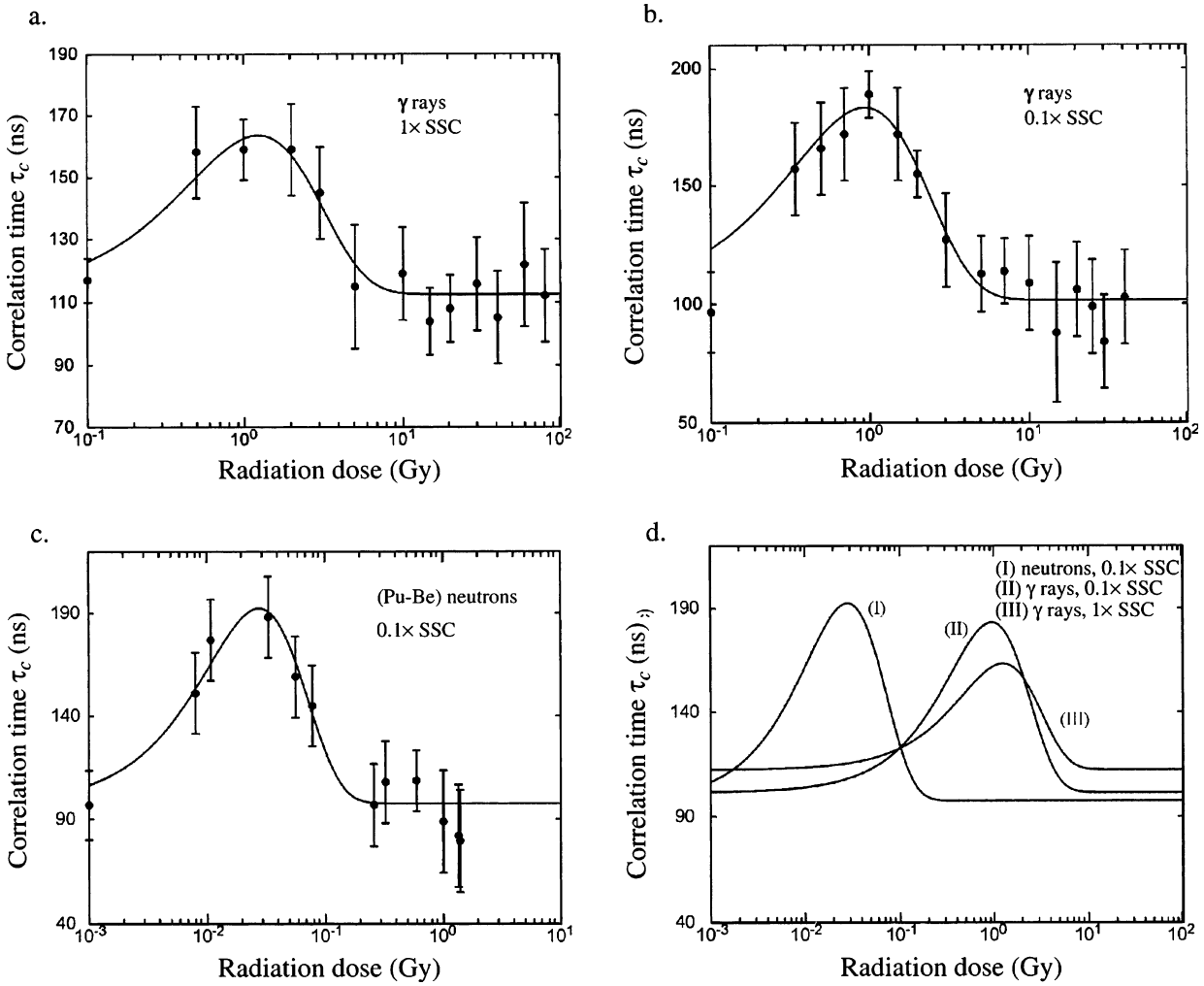

Figure 29. Rotational correlation time of calf thymus DNA as a function of radiation dose of γ-rays for salt concentrations of 1 and 0.1 SSC and as a function of radiation dose of neutrons at a concentration of 0.1 SSC. (1 SSC is 0.15 M sodium chloride and 0.0015 M sodium citrate). There is a maximum in the correlation time at certain doses, indicating an increased rigidity of the DNA structure at the maximum. The position of the maximum depends on the type of radiation (γ-rays or neutrons) and on the salt concentration. For details, see ref 98. Reprinted with permission from ref 98. Copyright 2003 Radiation Research.

Figure 30. In vivo ^{111}In PAC experiments on mice. Meares and Westmoreland[101] have used time-integrated PAC on ^{111}In-labeled compounds in living mice. The mouse was placed in the barrel of a slightly modified 60 mL syringe. Thereby, the time development of $^{111}In^{3+}$ bound to EDTA, citrate, chloride, and nitrilotriacetate could be followed in living mice.

nitrilotriacetic acid to 0.21 where indium was bound to macromolecules. The half-life of the vesicles in mice was estimated to be 10−13 h. Because liposomes are potential carriers of therapeutic and pharmacologically active agents, such studies can give important information on the lifetime of lipid vesicles of different lipid composition. The method of measuring the TIPAC was also used in a study of the effect of the modification of the surface of liposomes with oligosaccharides, in which the half-life of the degradation of the vesicles varied from 12 to 600 h depending on their composition.[103]

4.3.4.1.2. In Vivo Degradation of Liposomes in Rats. In vivo studies were expanded in a study focusing on liposomes as potential drug carriers to the liver and spleen.[104,105] The time-integrated angular perturbation factor, $\bar{G}_{22}$, of ^{111}In chelated by nitrilotriacteic acid inside the liposomes was 0.59 ± 0.02, whereas $\bar{G}_{22}$ of ^{111}In in bovine serum was 0.19 ± 0.02. Thus, it was possible to use the time-integrated perturbation factor as an indicator of the in vivo degree of degradation of liposomes by measuring $\bar{G}_{22}$ for blood samples as well as samples of liver and spleen taken from different rats that had been killed at various times after the injection of ^{111}In-nitrilotriacteic acid-loaded liposomes.[104] In this study, it was shown that the degradation depends on the lipid composition as well as the size of the vesicles. In a similar study, the effect of cholesterol on the degradation rate was investigated,[105] and it was found that cholesterol-containing liposomes are substantially more resistant to intracellular degradation than cholesterol free liposomes. In the latter studies, the PAC experiments were not carried out on the living rats but on samples taken from rats after they had been killed.

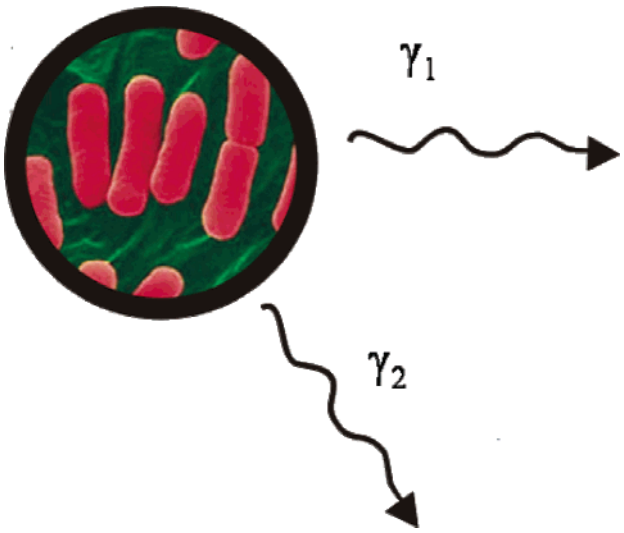

Figure 31. Fe/Mo nitrogenases and Mo storage proteins have been investigated in a number of in vivo and in vitro PAC studies.[106−109] The molybdenum uptake was studied in *A. vinelandii*, *K. pneumonia*, and *R. capsulatus*. The figure illustrates that bacteria have been grown on a medium with radioactive molybdenum, whereby this PAC isotope is incorporated into Mo-containing proteins.

4.3.4.2. In Vivo Studies of Molybdenum-Containing Proteins in Bacteria. Nitrogenases are important enzymes for nitrogen fixation and are classified according to their metal ion content. One class is the Fe/Mo-nitrogenases. This has been studied with time differential ^{99}Mo PAC spectroscopy in vivo and in vitro.[106−109] In the case of *Azotobacter vinelandii*, it was possible to grow the bacteria under conditions where the molybdenum was incorporated either preferentially into the Fe/Mo nitrogenase or into the Mo storage protein. The two proteins can be clearly distinguished by their quadrupole coupling constant, which was about 67 MHz for the MoFe protein and about 180 MHz for the Mo storage protein. *Klebsiella pneumoniae* and *Rhodobacter capsulatus* were also studied, and turned out to contain MoFe proteins with about the same quadrupole coupling constant as for *A. vinelandii*. These findings together with the possibility of studying the molybdenum uptake for different mutants offer a unique possibility in the future to follow the molybdenum uptake pathways.

4.3.5. Oriented Samples

If the sample is oriented such as in a single crystal or partly oriented such as in the case of molecules adhering to a surface, additional information can be obtained by recording spectra for different orientations of the sample with respect to the detectors. In a single crystal experiment, information on the full EFG tensor can be obtained, that is, five independent parameters, instead of the two (ω_0 and η) that can be obtained for randomly oriented samples. This is demonstrated for bis(imidazole)silver(I) nitrate crystals;[30] see Figure 32.

4.3.6. Proteins on Surfaces

This approach combines the advantages of PAC spectroscopy with the increased information that can be obtained with a sample of oriented molecules, for example, studies of a two-dimensional crystal of

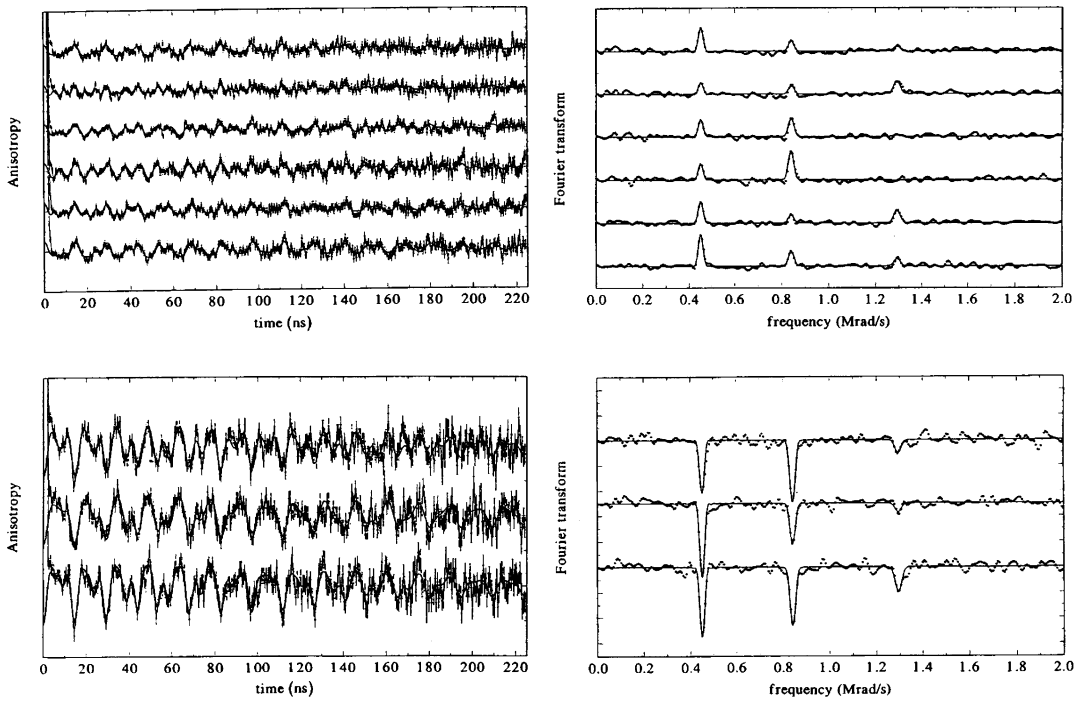

Figure 32. Single crystal ^{111}Ag PAC experiment on bis(imidazole)silver(I) nitrate.[30] Left: Stacked perturbation functions for different sample−detector orientations. Right: Fourier transforms of the perturbation functions. Although this is not directly biologically relevant, it is included in order to demonstrate the additional information that can be gained for oriented samples. As shown, the orientation does not change the frequencies, but the amplitude of each frequency depends on the orientation of the sample with respect to the detectors. Note that there is a typing error in the original figure, which has not been corrected here; Mrad/s should be Grad/s. Reprinted with permission from ref 30. Copyright 1999 American Physical Society.

proteins. This approach was used by Ctortecka et al.[110] to study stellacyanin (*R. vernicifera*), azurin (*P. aeruginosa*), and plastocyanin (*spinacea*) adsorbed on a surface. From the six independent detectors in a usual PAC camera, three planes can be formed (four detectors in each plane). Ctortecka et al. calculated $A_{22}G_{22}(t)$ for all three planes but were unable to observe any differences within the experimental accuracy, even though AFM indicated crystalline order for stellacyanin on MoS_2.[63]

5. Summary: Advantages and Limitations of PAC Spectroscopy

For the studies of biochemical problems, PAC spectroscopy offers a number of advantages, some of which have been illustrated by the examples given above.

(i) The coordination geometry at the site of a PAC isotope (e.g., a metal ion binding site in a protein) can be investigated in terms of possible coordinating ligands, ligand positions, and metal ion binding site flexibility.

(ii) The spectral parameters are extremely sensitive to changes in the first coordination sphere of the PAC isotope. In general, a movement of a ligand of 1−2° is detectable. (However, limitation number ii listed below should be noted.)

(iii) The rotational correlation times of molecules, which bind or can be labeled with a PAC isotope, can be measured. This allows for investigations of protein−protein and protein−membrane interactions, as well as global and internal dynamics of proteins.

(iv) It is possible to perform measurements at very low concentrations. The lower limit for ^{111m}Cd in metalloproteins is about 100 nM, limited by extraneous metal pollutions. In principle, only about 1 pmol of radioactive nuclei is required. Typical volumes are about 0.1−1 mL.

(v) It is possible to perform measurements on metal ion-containing enzymes during the active interconversion of substrate and product.

(vi) The total amplitude of the measured anisotropy, A_{22}^{eff}, is determined by nuclear properties and the geometry of the experimental setup. Thus, for a given setup, the sum of amplitudes, corresponding to different coordination geometries, must add up to this number. This is a useful check that no coordination geometries have been missed in the fitting procedure.

(vii) It is possible to determine rate constants for chemical exchange of the PAC isotope in analogy with chemical exchange in NMR but at a shorter time scale. For ^{111m}Cd, the typical time regime in which dynamic features can be studied is 0.1−100 ns. Details and an example can be found in the section on metallo β-lactamases, and the basic theory has been derived and can be found in the literature.[23−25] For dynamic situations that cannot easily be solved analytically, such as when the principal axis changes orientation, the spectra can be simulated by Monte Carlo methods.[21]

(viii) It is possible to perform measurements in liquid solution, frozen samples, solid state, on gel-bound material, and other vastly different physical situations.

(ix) The high transparency of biological material to γ-rays allows for noninvasive measurements in vivo on plants, animals, etc.

(x) The experimental setup allows mechanical stirring, or flow, of, for example, substrate past an immobilized enzyme.

(xi) Because of the very small amount of radioactive nuclei involved, it is possible to titrate multinuclear proteins from very small concentrations to stoichiometric concentrations. Thereby, sometimes making it possible to populate different sites or observe interactions and thus cooperativity of binding between the metal ions.

The limitations of the technique are:

(i) It is necessary to bind a suitable PAC isotope to the molecule of interest in stoichiometric or substoichiometric amounts; that is, the molecule must bind the PAC isotope strongly.

(ii) The spectral parameters do not uniquely determine the coordination geometry of the PAC isotope. That is, different structures can give rise to identical spectra. Typically, other chemical, spectroscopic, or structural information is used together with the PAC data, when interpretations in terms of structure are carried out.

(iii) Gas phase measurements are not feasible due to the rapid rotational motion of the molecules.

(iv) To perform measurements on catalytically active enzymes, the rate of the process must be low enough to ensure $[S] \geq K_M$ during the PAC measurement ([S] is the substrate concentration, and K_M is the Michaelis constant). The minimum time needed to obtain reasonable statistics in a ^{111m}Cd PAC experiment with a six detector setup is about 10 min.

(v) So-called after effects from the decay of the parent isotope can cause problems. If the parent isotope decays by isomeric transition (IT), after effects are normally not observed. A particularly unfavorable case is the one of EC, which is often followed by the emission of a number of Auger electrons, leaving the daughter isotope in a chemically unstable situation. That this can cause serious problems is illustrated in a comparison of ^{111m}Cd and ^{111}In experiments.[34]

6. Abbreviations

PAC, perturbed angular correlation of γ-rays; TIPAC, time-integrated perturbed angular correlation of γ-rays; EFG, electric field gradient; Grad, 10^9 radian/s = rad/ns; Mrad, 10^6 radian/s; MHz, 10^9 s^{-1}; NQI, nuclear quadrupole interaction; DTPA, diethylenetriaminepentaacetic acid; EDTA, ethylenediaminetetraacetic acid; LADH, liver alcohol dehydrogenase; DMSO, dimethyl sulfoxide; BASIL, Bauer's axially symmetric independent ligands; ESR, electron spin resonance; NMR, nuclear magnetic resonance; NQR, nuclear quadrupole resonance.

7. Acknowledgments

Rogert Bauer and Mikael Jensen, The Royal Veterinary and Agricultural University, Copenhagen,

Denmark, are both acknowledged for valuable discussions during the preparation of the manuscript. Professor Rogert Bauer passed away on April 15, 2004. His effort and enthusiasm in the development of applications of PAC spectroscopy to biology will be greatly missed, and we will miss him and his advice. This work was supported by the Danish Technical Research Council (Contract 26-00-0228) and the EU Research Training Network "Transient" (Contract HPRN-CT-1999-00095).

8. Appendix A: Theory of PAC Spectroscopy

The formalism of PAC can be found in the excellent review by Frauenfelder and Steffen.[3] Here, we will only present some of the main equations. For a nucleus decaying with the successive emission of two γ-rays, the probability of the second γ-ray being emitted in a direction given by the vector $\mathbf{k}_2$, at time, t, after the emission of the first γ-ray in direction, $\mathbf{k}_1$, is given by:[3]

$$P(\mathbf{k}_1,\mathbf{k}_2,t) \propto e^{-t/\tau_N}\, W(\mathbf{k}_1,\mathbf{k}_2,t) = e^{-t/\tau_N} \sum_{k_1 k_2} A_{k_1}(\gamma_1)\, A_{k_2}(\gamma_2)\, (2k_1+1)^{-1/2} (2k_2+1)^{-1/2} \sum_{N_1 N_2} G_{k_1 k_2}^{N_1 N_2}(t)\, Y_{k_1}^{N_1 *}(\theta_1,\varphi_1)\, Y_{k_2}^{N_2}(\theta_2,\varphi_2) \quad \text{(A.1)}$$

Here, τ_N denotes the lifetime of the intermediate level. The sum runs over even k_1 and k_2, and the range is from 0 to $k_{max} \leq \min(2L,2I)$, where L is the largest multipolarity for the corresponding γ-ray and I is the spin of the intermediate nuclear level. For example, the multipolarity of the first γ-ray emitted from ^{111m}Cd is 3 and of the second is 2, and the intermediate level has spin 5/2. In the case of an intermediate spin of 5/2, which is the case for most used PAC isotopes, the values of $k_{1,2}$ take the values of 0, 2, and 4 (at the most). The anisotropy coefficients A_{k_1} and A_{k_2} depend on the spin of the initial, intermediate, and final states of the decay, as well as the multipolarities of the γ-rays. Explicit formulas for the coefficients are given by Butz.[1,2] The sum over N_1 runs from $-k_1$ to $+k_1$ and N_2 runs from $-k_2$ to $+k_2$. Y_k^N are spherical harmonics and θ_i and φ_i are the polar and azimutal angles of the corresponding vector, $\mathbf{k}_i$.

The perturbation functions $G_{k_1 k_2}^{N_1 N_2}(t)$ are given by:

$$G_{k_1 k_2}^{N_1 N_2}(t) = \sum_{m_a m_b} (-1)^{2I+m_a+m_b} (2k_1+1)^{-1/2} (2k_2+1)^{-1/2} \cdot \begin{pmatrix} I & I & k_1 \\ m_a' & -m_a & N_1 \end{pmatrix} \begin{pmatrix} I & I & k_2 \\ m_b' & -m_b & N_2 \end{pmatrix} \langle m_b|\Lambda(t)|m_a\rangle \langle m_b'|\Lambda(t)|m_a'\rangle^* \quad \text{(A.2)}$$

Here

$$\begin{pmatrix} I & I & k_i \\ m_x' & -m_x & N_i \end{pmatrix}$$

are Wigner 3-j symbols and $|m_x\rangle$ represents the eigenfunction of the angular momentum operator, I^2 and I_z with eigenvalues $I(I+1)\hbar^2$ and $m_x\hbar$, respectively.

The interaction between the nucleus and the surroundings is reflected in the time evolution operator, $\Lambda(t)$. The matrix elements $\langle m_b|\Lambda(t)|m_a\rangle$ represent the probability that the nucleus is in state m_b at time t given that it was in state m_a at time 0. In the case of time-independent interactions, $\Lambda(t)$ is given by:

$$\Lambda(t) = e^{-i\,\hat{\mathbf{H}}\,t/\hbar} \quad \text{(A.3)}$$

where $\hat{\mathbf{H}}$ is the Hamiltonian describing the interaction of the nucleus in its intermediate state with the magnetic field and/or the EFG of its environment.

For a static NQI, the traceless part of the EFG is denoted $\bar{\bar{V}}$, and the axes are chosen such that $\bar{\bar{V}}$ is diagonal and $|V_{zz}| \geq |V_{yy}| \geq |V_{xx}|$. The parameters of the nucleus can be taken into account by defining:

$$\bar{\omega} = \frac{3eQ}{2[3I^2 - I(I+1)]\hbar}\bar{\bar{V}}$$

In that case, the NQI is characterized by $\omega_0 = |\omega_{zz}|$ and $\eta = (|V_{yy}| - |V_{xx}|)/|V_{zz}|$. The Hamiltonian for a static NQI can now be expressed in terms of the magnetic quantum numbers, m, in the following form:[1,2]

$$\begin{cases} H_{m,m} = \hbar\omega_0[3m^2 - I(I+1)]\dfrac{1}{6} \\ H_{m,m\pm 2} = \hbar\omega_0\eta[(I \mp m - 1)(I \mp m) \\ \qquad (I \pm m + 1)(I \pm m + 2)]^{1/2}\dfrac{1}{12} \end{cases} \quad \text{(A.4)}$$

For a general nondiagonal EFG, a unitary matrix, $\hat{\mathbf{U}}$, is required to diagonalize $\hat{\mathbf{H}}$ and the matrix elements of Λ become

$$\langle m_b|\Lambda(t)|m_a\rangle = \sum_n \langle n|m_b\rangle \times e^{-iE_n t/\hbar} \langle n|m_a\rangle \quad \text{(A.5)}$$

Here, the energies E_n denote the eigenvalues of $\hat{\mathbf{H}}$ and $\langle n|m_b\rangle$ are the matrix elements of $\hat{\mathbf{U}}$. Explicit analytic expressions of $\hat{\mathbf{U}}$ and E_n for magnetic interactions as well as NQIs are given by Butz.[1,2]

Often the investigated samples consist of randomly oriented molecules or randomly oriented microcrystals. This simplifies the above equations significantly. In this case, the correlation function is only a function of the angle and time between the two emitted γ-rays, θ:

$$W(\theta,t) = \sum_k A_k(1)\, A_k(2)\, G_{kk}(t)\, P_k(\cos\theta) \quad \text{(A.6)}$$

where $P_k(\cos\theta)$ is the Legendre polynomial and the function $G_{kk}(t)$ can be expressed in the form:

$$G_{kk}(t) = \frac{1}{2k+1} \sum_{N=-k}^{N=k} G_{kk}^{NN}(t) \quad \text{(A.7)}$$

Thus, the function $G_{22}(t)$ can be written as a sum over terms $e^{-i(E_n - E_{n'})t/\hbar}$ and therefore contains terms of $\cos(\omega t)$, where $\omega = (E_n - E_{n'})/\hbar$. For the particular case of a nucleus with an intermediate level of spin

5/2 in randomly oriented but otherwise identical static EFGs, $G_{22}(t)$ contains four terms:

$$G_{22}(t) = a_0 + a_1\cos(\omega_1 t) + a_2\cos(\omega_2 t) + a_3\cos(\omega_3 t) \quad \text{(A.8)}$$

9. Appendix B: The BASIL Semiempirical Method

The angular overlap model was originally developed for the calculation of energy splitting of the d levels in transition metal complexes (ref 28 and references therein) due to the interaction of the metal with the ligands. For the calculation of NQIs, however, not only are the energy changes required but also the changes of the wave function have to be known.

The AOM modified for NQI calculations by Bauer et al.[28] is in this paper referred to as the BASIL model for Bauers Axially Symmetric Independent Ligands. The assumptions in the model can be expressed as: (i) The NQI produced by a ligand is axially symmetric; that is, $V_{xx} = V_{yy}$, with the z-axis along the Cd−ligand bond. This means that σ-bonding but not π-bonding is taken into account. This assumption is not strictly necessary; that is, π-bonding can be included in the model. (ii) The metal−ligand interaction is described in the basis of p orbitals ($l = 1$), centered on cadmium, when calculating the NQI. The underlying idea is that the NQI originates from partial filling of cadmium 5p orbitals. (iii) The contributions to the NQI from different ligands are additive, i.e., a ligand−ligand interaction is not taken into account. It is implicitly assumed that the NQI from a given ligand does not depend on the bond length, within reasonable limits.

Within this modified AOM, each ligand can be assigned a characteristic interaction parameter, ω_l, the so-called partial NQI. In a fictitious complex with only one ligand, one would measure $\omega_0 = \omega_l$ and $\eta = 0$.

The partial NQI includes point charges on ligands, if they are positioned along the metal−ligand axis. Other ionic contributions to the EFG can also be included if their positions are known,[28] and they may give rise to a significant EFG due to polarization of the cadmium orbital. The ω_l values have been determined for several biologically relevant ligands;[28] see Table 4.[27,111]

Table 4. Partial NQI Parameters for Biologically Relevant Ligands

ligand	partial NQI (Mrad/s)	ref
sulfate	250 (4)	28
amine	139 (4)	28
carboxylate (monodentate)	245 (5)	28
carboxylate (bidentate)	175 (5)	28
imidazole (histidine)	95 (4)	28
chloride	231 (5)	28
acyl (carbonyl)	161 (8)	28
water	207 (11)	28
hydrazine	190 (7)	28
thiocyl	330 (5)	28
mercapto (cysteine)	300 (2)	111
thioester (methionine)	102	112
hydroxyl (value based on calculations)	349	40

The reliability of the model can be evaluated by comparing measured NQIs with calculated NQIs. This is done for a number of structures in Table 5. Note that the calculations are generally performed on structures of the native zinc- or copper ion-containing proteins, whereas the measurements are carried out on cadmium ion-containing structures. Thus, deviations can be due to limitations of the model as well as structural changes induced by the metal ion substitution.

10. Appendix C: An Example of the BASIL Method Applied to Blue Copper Proteins

The purpose of this appendix is to provide an example of the application of the BASIL model that is so simple that it can be carried out by hand. If we approximate the metal ion binding site in blue copper proteins by a planar, symmetric structure, consisting of one cysteine and two histidines coordinating, it becomes particularly simple to apply the semiempirical model.

The partial NQIs, ω_l, of cysteine and histidine are 300 and 95 Mrad/s, respectively (see Table 4). A ligand positioned in the direction of the unit vector (x,y,z), in a coordinate system with cadmium at the origin, contributes to the total NQI tensor, $\bar{\omega}$, by:

$$\bar{\omega} = \omega_l \begin{pmatrix} (3x^2-1)/2 & 3xy/2 & 3xz/2 \\ 3xy/2 & (3y^2-1)/2 & 3yz/2 \\ 3xz/2 & 3yz/2 & (3z^2-1)/2 \end{pmatrix} \quad \text{(C.1)}$$

In the BASIL model, the total NQI tensor is simply the sum of the contributions from the individual ligands. In azurin from *P. aeruginosa*, the three ligands form the angles: $\alpha(N_{46} - N_{117}) = 103°$, $\alpha(N_{46} - S_{112}) = 134°$, and $\alpha(S_{112} - N_{117}) = 123°$. The sum of these three angles is 360°, and the structure is thus planar. However, it is not quite symmetric. To make it simple to do the calculation, we will assume that the structure is planar with $\alpha(N_{46} - N_{117}) = 103°$ and $\alpha = \alpha(N_{46} - S_{112}) = \alpha(S_{112} - N_{117}) = 128.5°$. We will further choose the coordinate system such that the cysteine is located on the z-axis and the two histidines lie in the $x-z$-plane. The unit vector of the cysteine is thus (0,0,1), and the unit vector of the two histidines is $[\pm\sin(\alpha),0,\cos(\alpha)]$. The resulting expression of $\bar{\bar{\omega}}$ is

$$\bar{\bar{\omega}} = 300\ \text{Mrad/s} \begin{pmatrix} -1/2 & 0 & 0 \\ 0 & -1/2 & 0 \\ 0 & 0 & 1 \end{pmatrix} + 95\ \text{Mrad/s} \begin{bmatrix} (3\sin^2(\alpha)-1)/2 & 0 & \sin(\alpha)\cos(\alpha) \\ 0 & -1/2 & 0 \\ \sin(\alpha)\cos(\alpha) & 0 & (3\cos^2(\alpha)-1)/2 \end{bmatrix} + 95\ \text{Mrad/s} \begin{bmatrix} (3\sin^2(\alpha)-1)/2 & 0 & -\sin(\alpha)\cos(\alpha) \\ 0 & -1/2 & 0 \\ -\sin(\alpha)\cos(\alpha) & 0 & (3\cos^2(\alpha)-1)/2 \end{bmatrix} \quad \text{(C.2)}$$

This matrix is diagonal with the diagonal elements: $\omega_{xx} = -300/2 + 2{\cdot}95 \cdot [3\sin^2(128.5) - 1]/2$, $\omega_{yy} =$

Table 5. Comparison of PAC Measurements and BASIL Calculations[a]

	PAC experiment			AOM calculation			
	Mrad/s						
complex/protein	$\lvert\omega_{xx}\rvert$	$\lvert\omega_{yy}\rvert$	$\lvert\omega_{zz}\rvert$	$\lvert\omega_{xx}\rvert$	$\lvert\omega_{yy}\rvert$	$\lvert\omega_{zz}\rvert$	refs[f]
Cd(L-Glu)(H_2O)·H_2O[b]	25	102	127(1)	18	104	122	28, 113
Cd-D-penicillamine[c]	90	199	289(3)	110	137	247	111, 114, 115
horse LADH	8	262	270(4)	53	214	267	18, 116
horse LADH·NADH[d]	19	314	333(1)	52	253	305	18, 116
	34	292	326(1)				
carboxypeptidase A	52	103	155(1)	44	104	150	65, 66
human carbonic anhydrase	30	84	114(4)	48	64	112	117, 118
bovine super oxide dismutase (zinc site)	47	100	147.2(6)	54	85	139	119, 120
azurin[e] (*P. aeruginosa*)	81	257	337.7(2)	71	243	314	27, 43

[a] The ω_{ii} values are the eigenvalues of the NQI tensor. The sign of the ω_{ii} values is not measured; therefore, only the absolute values are presented here. The experimental uncertainty on $\lvert\omega_{xx}\rvert$ and $\lvert\omega_{yy}\rvert$ can be derived from the uncertainties in η and $\lvert\omega_{zz}\rvert$ and will generally be in the order of the uncertainty on $\lvert\omega_{zz}\rvert$. [b] Aqua(L-glutamato)cadmium(II) monohydrate. [c] D-Penicillaminatocadmium(II). [d] Two very similar NQIs were observed. [e] Assuming a three-coordinate metal ion binding site (His46, His117, and Cys112). [f] The first reference is for the PAC work, and the second reference is for the structure used in the BASIL calculation.

$-300/2 - 95 = -245$ Mrad/s, and $\omega_{zz} = 300 + 2\cdot95 \cdot [3\cos^2(128.5) - 1]/2 = 315.4$ Mrad/s. The largest diagonal element, ω_0, is the latter with the numerical value of 315.4 Mrad/s; the second largest element is -245 Mrad/s, and the smallest is -70.4 Mrad/s. The asymmetry is thus $\eta = (245 - 70.4)/315.4 = 0.554$. Note that in this case ω_0 reflects the EFG in the direction of the cysteine, whereas ω_{yy} reflects the EFG in the direction perpendicular to the plane formed by the three ligands. Further discussion of the semiempirical model used on a blue copper protein is given in Danielsen et al.[112] Although the mathematical task of calculating ω_0 and η is limited, it is also clearly an advantage to have the calculation computerized. A public version for such calculations is given on a web site by Danielsen.[41] Using the real crystal structure yields an ω_0 of 316.1 Mrad/s and η of 0.550; thus, our simplified structure was a good approximation to the real structure. The experimental result of the ^{111m}Cd PAC spectra on azurin from *P. aeruginosa* was ω_0 of 337.7(2) Mrad/s and η of 0.522(1). There is not a perfect match between the calculated and the measured values of ω_0. However, considering the simplicity of the model, it comes rather close. One possible deviation is that the partial NQIs that are input parameters in the model do not allow for Cd−ligand bond length dependence. If the distances are shorter in this low coordination number structure than in the model complexes used for determining the partial NQIs, then it is likely that the interaction parameters should be higher. An increase by 7% is enough to account for the minor deviation. This example also gives a good idea of the limited accuracy of the model. Calculations based on structures where the methionine is coordinating gives a calculated NQI of ω_0 of 286.1 Mrad/s and η of 0.151, and if the glycine 45 is also assumed to coordinate, the model calculation yields ω_0 of 207.9 Mrad/s and η of 0.916[27] (the related Fourier-transformed PAC spectra are illustrated in Figure 8).

The orientation of the principal axis of the EFG can also easily be calculated for the symmetric molecule. If the two histidines and the cysteine are forming a planar symmetric structure as described above, the effect of adding axial ligands is calculated simply by adding extra terms in eq C.2. Adding a methionine as an axial ligand with partial NQI of 102 Mrad/s changes the diagonal element perpendicular to the plane to $\omega_\perp = -245 + 102$ Mrad/s $= -143$ Mrad/s and in the plane in the direction of the cysteine: $\omega_\parallel = 315.4 - 1/2\cdot102$ Mrad/s $= 264.4$ Mrad/s. The last diagonal element with the axis in the plane and perpendicular to the cysteine thus becomes $\omega_= = -121.4$ Mrad/s. In this case, the Cd−Cys axis

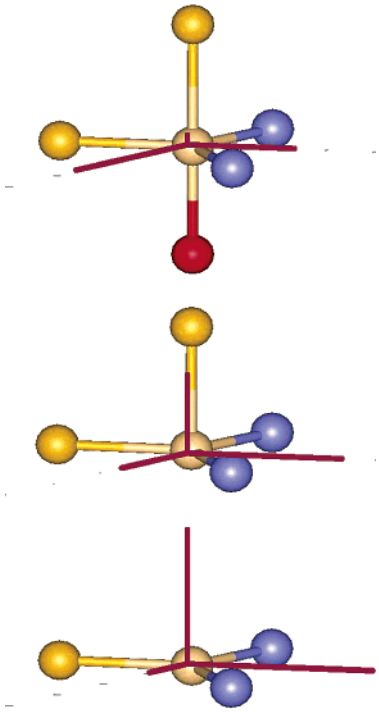

Figure 33. Magnitude of the eigenvalues and orientation of the principal axis of the EFG for azurin model systems. The figure illustrates how adding extra ligands affects the magnitude of the eigenvalues of the EFG. The coordinating ligands are the same as in Figure 8 but with the axial ligands on the axis for simplicity, because in this case, the principal axis coordinate system is the same for all three model systems. Calculations are carried out using the BASIL model (see the text of appendix C). In the three-coordinated and four-coordinated structures, the principal axis with the largest eigenvalue (*z*-axis) lies along the Cd−Cys bond, and the *y*-axis is perpendicular to the Cys, his, his plane. In the five-coordinated structure, the *z*-axis lies in the plane and perpendicular to the Cd−Cys bond, and the *y*-axis lies along the Cd−Cys bond.

is still the *z*-axis and the axis perpendicular to the plane is still the *y*-axis (see Figure 33). If an additional carbonyl group from the backbone of glycine 45 is added opposite to the methionine, the diagonal elements become $\omega_{\perp} = 18$ Mrad/s, $\omega_{\parallel} = -183.9$ Mrad/s, and $\omega_{=} = -201.9$ Mrad/s. Note that now the *z*-axis lies in the Cys-His-His plane and perpendicular to the Cd-cysteine bond.

11. References

(1) Butz, T. *Hyperfine Interact.* **1989**, *52*, 189.
(2) Butz, T. *Hyperfine Interact.* **1992**, *73*, 387.
(3) Frauenfelder, H.; Steffen, R. M. *Alpha-, Beta and Gamma-Ray Spectroscopy*; North-Holland: Amsterdam, 1965; p 997.
(4) Haas, H.; Shirley, D. A. *J. Chem. Phys.* **1973**, *58*, 3339.
(5) Rinneberg, H. H. *At. Energy Rev.* **1979**, *172*, 477.
(6) Lerf, A.; Butz, T. *Hyperfine Interact.* **1987**, *36*, 275.
(7) Lerf, A.; Butz, T. *Angew. Chem.-Int. Ed. Engl.* **1987**, *26*, 110.
(8) Shirley, D. A.; Haas, H. *Annu. Rev. Phys. Chem.* **1972**, *23*, 385.
(9) Bauer, R. *Q. Rev. Biophys.* **1985**, *18*, 1.
(10) Bauer, R.; Bjerrum, M. J.; Danielsen, E.; Kofod, P. *Acta Chem. Scand.* **1991**, *45*, 593.
(11) Feiock, F. D.; Johnson, W. R. *Phys. Rev.* **1969**, *187*, 39.
(12) Hamilton, D. R. *Phys. Rev.* **1940**, *58*, 122.
(13) Brady, E. L.; Deutsch, M. *Phys. Rev.* **1947**, *72*, 870.
(14) Goertzel, G. *Phys. Rev.* **1946**, *70*, 897.
(15) Aeppli, H.; Bishop, A. S.; Frauenfelder, H.; Walter, M.; Zunti, W. *Phys. Rev.* **1951**, *82*, 550.
(16) Frauenfelder, H. *Phys. Rev.* **1951**, *82*, 549.
(17) Leipert, T. K.; Baldeschwieler, J. D.; Shirley, D. A. *Nature* **1968**, *220*, 907.
(18) Hemmingsen, L.; Bauer, R.; Bjerrum, M. J.; Zeppezauer, M.; Adolph, H. W.; Formicka, G.; Cedergren Zeppezauer, E. *Biochemistry* **1995**, *34*, 7145.
(19) Perrin, F. *J. Phys. Radium* **1934**, *5*, 497.
(20) Danielsen, E.; Bauer, R. *Hyperfine Interact.* **1990**, *62*, 311.
(21) Danielsen, E.; Jørgensen, L. E.; Sestoft, P. *Hyperfine Interact.* **2002**, *142*, 607.
(22) Danielsen, E.; Jørgensen, L. E.; Sestoft, P. PAC-simulator. www.matfys.kvl.dk/pacsimulator, 2001.
(23) Bauer, R. Ph.D. thesis, University of Copenhagen, Niels Bohr Institute, 1976.
(24) Winkler, H.; Gerdau, E. *Z. Phys.* **1973**, *262*, 363.
(25) Clauser, M. J. *Phys. Rev. B* **1971**, *3*, 3748.
(26) Butz, T.; Saibene, S.; Fraenzke, T.; Weber, M. *Nucl. Instrum. Methods Phys. Res., Sect. A* **1989**, *284*, 417.
(27) Danielsen, E.; Bauer, R.; Hemmingsen, L.; Andersen, M. L.; Bjerrum, M. J.; Butz, T.; Tröger, W.; Canters, G. W.; Hoitink, C. W. G.; Karlsson, G.; Hansson, Ö.; Messerschmidt, A. *J. Biol. Chem.* **1995**, *270*, 573.
(28) Bauer, R.; Jensen, S. J.; Schmidt-Nielsen, B. *Hyperfine Interact.* **1988**, *39*, 203.
(29) Hemmingsen, L.; Ryde, U. *J. Phys. Chem.* **1996**, *100*, 4803.
(30) Hansen, B.; Bukrinsky, J. T.; Hemmingsen, L.; Bjerrum, M. J.; Singh, K.; Bauer, R. *Phys. Rev. B* **1999**, *59*, 14182.
(31) Bauer, R.; Christensen, C.; Larsen, E. *J. Chem. Phys.* **1979**, *70*, 4117.
(32) Jørgensen, L. E.; Ubbink, M.; Danielsen, E. *J. Biol. Inorg. Chem.* **2004**, *9*, 27.
(33) Bauer, R.; Danielsen, E.; Hemmingsen, L.; Bjerrum, M. J.; Hansson, Ö.; Singh, K. *J. Am. Chem. Soc.* **1997**, *119*, 157.
(34) Bauer, R.; Atke, A.; Danielsen, E.; Marcussen, J.; Olsen, C. E.; Rehfeld, J.; Saermark, T.; Schneider, D.; Vilhardt, H.; Zeppezauer, M. *Appl. Radiat. Isot.* **1991**, *42*, 1015.
(35) Pyykkö, P. *Z. Naturforsch., A: Phys. Sci.* **1992**, *47*, 189.
(36) Antony, J.; Hansen, B.; Hemmingsen, L.; Bauer, R. *J. Phys. Chem. A* **2000**, *104*, 6047.
(37) Ryde, U.; Hemmingsen, L. *J. Biol. Inorg. Chem.* **1997**, *2*, 567.
(38) Dufek, P.; Blaha, P.; Schwarz, K. *Phys. Rev. Lett.* **1995**, *75*, 3545.
(39) Hemmingsen, L.; Bauer, R.; Bjerrum, M. J.; Schwarz, K.; Blaha, P.; Andersen, P. *Inorg. Chem.* **1999**, *38*, 2860.
(40) Hemmingsen, L.; Ryde, U.; Bauer, R. *Z. Naturforsch., A: Phys. Sci.* **1999**, *54*, 422.
(41) Danielsen, E. AOM-calculator. http://www.matfys.kvl.dk/~eva/aom.html, 1999.
(42) Singh, H.; Binarh, H. S.; Ghumman, S. S.; Sahota, H. S. *Appl. Radiat. Isot.* **1990**, *41*, 797.
(43) Nar, H.; Messerschmidt, A.; Huber, R.; Vandekamp, M.; Canters, G. W. *J. Mol. Biol.* **1991**, *221*, 765.
(44) Adman, E. T.; Jensen, L. H. *Isr. J. Chem.* **1981**, *21*, 8.
(45) Tröger, W.; Butz, T. *Hyperfine Interact.* **2000**, *129*, 511.
(46) Butz, T.; Tröger, W. *Bioinorganic Chemistry, Transition Metals in Biology and Their Coordination Chemistry*; Wiley: Weinheim, 1997; Chapter 9, p 302.
(47) Danielsen, E.; Scheller, H. V.; Bauer, R.; Hemmingsen, L.; Bjerrum, M. J.; Hansson, Ö. *Biochemistry* **1999**, *38*, 11531.
(48) Xue, Y. F.; Ökvist, M.; Hansson, Ö.; Young, S. *Protein Sci.* **1998**, *7*, 2099.
(49) Tröger, W.; Lippert, C.; Butz, T.; Sigfridsson, K.; Hansson, Ö.; McLaughlin, E.; Bauer, R.; Danielsen, E.; Hemmingsen, L.; Bjerrum, M. J. *Z. Naturforsch. A: Phys. Sci.* **1996**, *51*, 431.
(50) Drepper, F.; Hippler, M.; Nitschke, W.; Haehnel, W. *Biochemistry* **1996**, *35*, 1282.
(51) Messerschmidt, A.; Ladenstein, R.; Huber, R.; Bolognesi, M.; Avigliano, L.; Petruzzelli, R.; Rossi, A.; Finazziagro, A. *J. Mol. Biol.* **1992**, *224*, 179.
(52) Butz, T.; Tröger, W.; Messerschmidt, A.; Thoenes, U.; Huber, R. *Hyperfine Interact.* **1993**, *80*, 1127.
(53) Butz, T. *Hyperfine Interact.* **1993**, *80*, 1079.
(54) Tröger, W.; Butz, T.; Danielsen, E.; Bauer, R.; Thoenes, U.; Messerschmidt, A.; Huber, R.; Canters, G. W.; den Blaauwen, T. *Hyperfine Interact.* **1993**, *80*, 1133.
(55) Piontek, K.; Antorini, M.; Choinowski, T. *J. Biol. Chem.* **2002**, *277*, 37663.
(56) Messerschmidt, A.; Rossi, A.; Ladenstein, R.; Huber, R.; Bolognesi, M.; Gatti, G.; Marchesini, A.; Petruzzelli, R.; Finazziagro, A. *J. Mol. Biol.* **1989**, *206*, 513.
(57) Vallee, B. L. *Zinc Enzymes*; Birkhäuser: Boston, 1986; Chapter 1, p 1.
(58) Bertini, I.; Luchinat, C. *Bioinorganic Chemistry*; University Science Books: Mill Valley, 1994; Chapter 2, p 37.
(59) Carfi, A.; Duee, E.; Paul-Soto, R.; Galleni, M.; Frere, J. M.; Dideberg, O. *Acta Crystallogr., Sect. D: Biol. Crystallogr.* **1998**, *54*, 47.
(60) Hemmingsen, L.; Damblon, C.; Antony, J.; Jensen, N.; Adolph, H. W.; Wommer, S.; Roberts, G. C. K.; Bauer, R. *J. Am. Chem. Soc.* **2001**, *123*, 10329.
(61) Paul-Soto, R.; Zeppezauer, M.; Adolph, H. W.; Galleni, M.; Frere, J. M.; Carfi, A.; Dideberg, O.; Wouters, J.; Hemmingsen, L.; Bauer, R. *Biochemistry* **1999**, *38*, 16500.
(62) Damblon, C.; Jensen, M.; Ababou, A.; Barsukov, I.; Papamicael, C.; Schofield, C. J.; Olsen, L.; Bauer, R.; Roberts, G. C. K. *J. Biol. Chem.* **2003**, *278*, 29240.
(63) Tröger, W. Habilitation thesis, Universität Leipzig, 2000.
(64) Jensen, A. F.; Bukrinsky, J. T.; Bjerrum, M. J.; Larsen, S. *J. Biol. Inorg. Chem.* **2002**, *7*, 490.
(65) Bauer, R.; Danielsen, E.; Hemmingsen, L.; Sorensen, M. V.; Ulstrup, J.; Friis, E. P.; Auld, D. S.; Bjerrum, M. J. *Biochemistry* **1997**, *36*, 11514.
(66) Rees, D. C.; Howard, J. B.; Chakrabarti, P.; Yeates, T.; Hsu, B. T.; Hardman, K. D.; Lipscomb, W. N. *Zinc Enzymes*; Birkhäuser: Boston, 1986; p 155.
(67) Denisov, V. P.; Halle, B. *J. Am. Chem. Soc.* **1995**, *117*, 8456.
(68) Eriksson, A. E.; Jones, T. A.; Liljas, A. *Proteins: Struct. Funct., Genet.* **1988**, *4*, 274.
(69) Bauer, R.; Limkilde, P.; Johansen, J. T. *Biochemistry* **1976**, *15*, 334.
(70) Bauer, R.; Johansen, J.; Limkilde, P. *Hyperfine Interact.* **1978**, *4*, 906.
(71) Bauer, R.; Limkilde, P.; Johansen, J. T. *Carlberg Res. Commun.* **1977**, *42*, 325.
(72) Kannan, K. K.; Notstrand, B.; Fridborg, K.; Lovgren, S.; Ohlsson, A.; Petef, M. *Proc. Natl. Acad. Sci. U.S.A.* **1975**, *72*, 51.
(73) Liljas, A.; Lovgren, S.; Bergsten, P. C.; Carlbom, U.; Petef, M.; Waara, I.; Strandberg, B.; Fridborg, K.; Jarup, L.; Kannan, K. K. *Nat. New Biol.* **1972**, *235*, 131.
(74) Lanir, A.; Gradstajn, S.; Navon, G. *Biochemistry* **1975**, *14*, 242.
(75) Lindskog, S.; Coleman, J. E. *Proc. Natl. Acad. Sci. U.S.A.* **1973**, *70*, 2505.
(76) Lindskog, S.; Henderson, L. E.; Kannan, K. K.; Liljas, A.; Nyman, P. O.; Strandberg, B. *Enzymes* **1971**, 587.
(77) Khalifah, R. G. *J. Biol. Chem.* **1971**, *246*, 2561.
(78) Rubach, J. K.; Ramaswamy, S.; Plapp, B. V. *Biochemistry* **2001**, *40*, 12686.
(79) Kvassman, J.; Pettersson, G. *Eur. J. Biochem.* **1979**, *100*, 115.
(80) Meijers, R.; Morris, R. J.; Adolph, H. W.; Merli, A.; Lamzin, V. S.; Cedergren-Zeppezauer, E. S. *J. Biol. Chem.* **2001**, *276*, 9316.
(81) Yang, A. H. W.; MacGillivray, R. T. A.; Chen, J.; Luo, Y. G.; Wang, Y. L.; Brayer, G. D.; Mason, A. B.; Woodworth, R. C.; Murphy, M. E. P. *Protein Sci.* **2000**, *9*, 49.
(82) Appel, H.; Duffield, J.; Taylor, D. M.; Then, G. M.; Thies, W. G. *Hyperfine Interact.* **1987**, *35*, 957.
(83) Appel, H.; Brownmason, A.; Neumüller, M.; Schwab, F.; Taylor, D. M.; Thies, W. G. *Hyperfine Interact.* **1990**, *61*, 1223.
(84) Schwab, F. J.; Appel, H.; Neu, M.; Thies, W. G. *Eur. Biophys. J. Biophys. Lett.* **1992**, *21*, 147.
(85) Schwab, F. J.; Appel, H.; Neu, M.; Thies, W. G. *Hyperfine Interact.* **1993**, *80*, 1155.
(86) Schwab, F. J.; Appel, H.; Mason, A. B.; Neu, M.; Thies, W. G. *Biometals* **1993**, *6*, 193.

(87) Appel, H.; Duffield, J.; Taylor, D. M.; Then, G. M.; Thies, W. G. *J. Inorg. Biochem.* **1987**, *31*, 229.
(88) Appel, H.; Neumüller, M.; Schwab, F.; Taylor, D. M.; Thies, W. G. *Hyperfine Interact.* **1990**, *61*, 1219.
(89) Then, G. M.; Appel, H.; Duffield, J.; Taylor, D. M.; Thies, W. G. *J. Inorg. Biochem.* **1986**, *27*, 255.
(90) Becker, G.; Appel, H.; Neu, M.; Schwab, F. J.; Thies, W. G. *Hyperfine Interact.* **1993**, *80*, 1161.
(91) Silver, S.; Misra, T. K. *Annu. Rev. Microbiol.* **1988**, *42*, 717.
(92) Tröger, W. *Hyperfine Interact.* **1999**, *120/121*, 117.
(93) Christou, G.; Folting, K.; Huffman, J. C. *Polyhedron* **1984**, *3*, 1247.
(94) Vis, R. D.; Bos, A. J. J.; Idzenga, S.; Verheul, H. *Nucl. Instrum. Methods* **1979**, *163*, 265.
(95) Kalfas, C. A.; Sideris, E. G.; El-kateb, S.; Martin, P. W.; Kuhnlein, U. *Chem. Phys. Lett.* **1980**, *73*, 311314.
(96) Kalfas, C. A.; Sideris, E. G.; Loukakis, G. K.; Anagnostopouloukonsta, A. *J. Non-Cryst. Solids* **1994**, *172*, 1121.
(97) Tsoulou, E.; Kalfas, C. A.; Sideris, E. G. *Radiat. Res.* **2001**, *156*, 181.
(98) Tsoulou, E.; Kalfas, C. A.; Sideris, E. G. *Radiat. Res.* **2003**, *159*, 33.
(99) Forssen, E. A. *Adv. Drug Delivery Rev.* **1997**, *24*, 133.
(100) Baldeschwieler, J. D.; Schmidt, P. G. *Chemtech* **1997**, *27*, 34.
(101) Meares, C. F.; Westmoreland, D. G. *Cold Spring Harbor Symp. Quant. Biol.* **1971**, *36*, 511.
(102) Hwang, K. J.; Mauk, M. R. *Proc. Natl. Acad. Sci. U.S.A.* **1977**, *74*, 4991.
(103) Mauk, M. R.; Gamble, R. C.; Baldeschwieler, J. D. *Science* **1980**, *207*, 309.
(104) Derksen, J. T. P.; Baldeschwieler, J. D.; Scherphof, G. L. *Proc. Natl. Acad. Sci. U.S.A.* **1988**, *85*, 9768.
(105) Roerdink, F. H.; Regts, J.; Handel, T.; Sullivan, S. M.; Baldeschwieler, J. D.; Scherphof, G. L. *Biochim. Biophys. Acta* **1989**, *980*, 234.
(106) Dong, M. L.; Huang, J. F.; Du, H. S.; Li, J. H.; Du, S. B.; Luo, A. L.; Jiang, Y.; Zhang, C. H. *J. Radioanal. Nucl. Chem.* **1996**, *205*, 261.
(107) Mottner, P.; Butz, T.; Lerf, A.; Erfkamp, J.; Schneider, K.; Müller, A. *Biochim. Biophys. Acta* **1993**, *1164*, 311.
(108) Müller, A.; Suer, W.; Pohlmann, C.; Schneider, K.; Thies, W. G.; Appel, H. *Eur. J. Biochem.* **1997**, *246*, 3311.
(109) Pohlmann, C.; Appel, H.; Thies, W. G.; Müller, A.; Schneider, K.; Suer, W. *Hyperfine Interact.* **1999**, *121*, 731.
(110) Ctorecka, B.; Hartmann, V.; Tröger, W.; Lösche, M.; Butz, T. Condensed matter studies by nuclear methods. In *Proceedings of the XXXII Zakopane School of Physics*; Görlich, E. A., Latka, K., Eds.; Institute of Physics, Jagiellonian University and Niewodniczanski Institute of Nuclear Physics: Krakow, 1997; p 137.
(111) Bauer, R.; Adolph, H. W.; Andersson, I.; Danielsen, E.; Formicka, G.; Zeppezauer, M. *Eur. Biophys. J.* **1991**, *20*, 215.
(112) Danielsen, E.; Bauer, R.; Hemmingsen, L.; Bjerrum, M. J.; Butz, T.; Tröger, W.; Canters, G. W.; den Blaauwen, T.; van Pouderoyen, G. *Eur. J. Biochem.* **1995**, *34*, 554.
(113) Flook, R. J.; Freeman, H. C.; Scudder, M. L. *Acta Crystallogr., Sect. B: Struct. Sci.* **1977**, *33*, 801.
(114) Freeman, H. C.; Huq, F.; Stevens, G. N. *J. Chem. Soc. Chem. Commun.* **1976**, 90.
(115) Leligny, H.; Monier, J. C. *Acta Crystallogr., Sect. B: Struct. Sci.* **1975**, *B 31*, 728.
(116) Eklund, H.; Jones, T. A.; Schneider, G. *Zinc Enzymes*; Birkhäuser: Boston, 1986; Chapter 7, p 377.
(117) Bauer, R. *Biological Application of Perturbed Angular Correlation*; Academic Press Copenhagen: Copenhagen, 1992.
(118) Errikson, E. A.; Jones, T. A.; Liljas, A. *Zinc Enzymes*; Birkhäuser: Boston, 1986; Chapter 23, p 317.
(119) Bjerrum, M. J.; Bauer, R.; Danielsen, E.; Kofod, P. *Free Radical Res. Commun.* **1991**, *12-3*, 297.
(120) Tainer, J. A.; Getzoff, E. D.; Beem, K. M.; Richardson, J. S.; Richardson, D. C. *J. Mol. Biol.* **1982**, *160*, 181.
(121) Firestone, R. B.; Shirley, V. S.; Baglin, C. M.; Chu, S. Y. F. *Table of Isotopes*; Whiley: Chirchester, 1996.
(122) Bauer, R.; Limkilde, P.; Glomset, O. *Phys. Rev. Lett.* **1974**, *32*, 340.
(123) Demille, G. R.; Larlee, K.; Livesley, D. L.; Mailer, K. *Chem. Phys. Lett.* **1979**, *64*, 534.
(124) Bauer, R.; Christensen, C.; Johansen, J. T.; Bethune, J. L.; Vallee. *Biochem. Biophys. Res. Commun.* **1979**, *90*, 679.
(125) Bauer, R.; Bjerrum, M.; Danielsen, E.; Friis, E.; Hammerstad, J. M.; Hemmingsen, L.; Pedersen, M. V.; Ulstrup, J. *Protein Folds: A Distance Based Approach*; CRC Press: Boca Raton, FL, 1996.
(126) Bauer, R.; Demeter, I.; Hasemann, V.; Johansen, J. T. *Biochem. Biophys. Res. Commun.* **1980**, *94*, 1296.
(127) Bauer, R.; Bjerrum, M.; Danielsen, E.; Kofod, P. *Hyperfine Interact.* **1990**, *61*, 1201.
(128) Hemmingsen, L.; Bauer, R.; Bjerrum, M. J.; Adolph, H. W.; Zeppezauer, M.; Cedergren Zeppezauer, E. *Eur. J. Biochem.* **1996**, *35*, 546.
(129) Hemmingsen, L.; Hansen, S. *Z. Naturforsch., Sect. A: Phys. Sci.* **1996**, *51*, 422.
(130) Carvalho, E.; Gothe, P. O.; Bauer, R.; Danielsen, E.; Hemmingsen, L. *Eur. J. Biochem.* **1995**, *34*, 780.
(131) de Seny, D.; Heinz, U.; Wommer, S.; Kiefer, M.; Meyer-Klaucke, W.; Galleni, M.; Frere, J. M.; Bauer, R.; Adolph, H. W. *J. Biol. Chem.* **2001**, *276*, 45065.
(132) Smith. F. A.; Martin, P. W.; Shukri, A. *Hyperfine Interact.* **1985**, *23*, 375.
(133) Tröger, W.; Ctortecka, B.; Faller, P.; Vasak, M. *J. Inorg. Biochem.* **2001**, *86*, 460.
(134) Vasak, M.; Bauer, R. *J. Am. Chem. Soc.* **1981**, *104*, 3226.
(135) Danielsen, E.; Kroes, S. J.; Canters, G. W.; Bauer, R.; Hemmingsen, L.; Singh, K.; Messerschmidt, A. *Eur. J. Biochem.* **1997**, *250*, 249.
(136) Holm, J. K.; Hemmingsen, L.; Bubacco, L.; Salvato, B.; Bauer, R. *Eur. J. Biochem.* **2000**, *267*, 1754.
(137) Tröger, W.; Ctortecka, B.; Faller, P.; Decker, H. *Z. Naturforsch., Sect. A: Phys. Sci.* **2002**, *57*, 623.
(138) Mekata, M.; Hamada, E. S. Y.; Sugiura, S.; Kawamura, M. *Hyperfine Interact.* **1990**, *61*, 1179.
(139) Mullins, O. C.; Kaplan, M. *J. Chem. Phys.* **1983**, *79*, 4475.
(140) Wang, Y. X.; Ni, X. B.; Chen, W. B.; Xu, J. L.; Sun, C. W.; Yin, D. Z.; Ding, S. *Biol. Trace Elem. Res.* **1989**, *22*, 1.
(141) Marsden, P. J.; Smith, F. A.; Evans, R. W. *Appl. Radiat. Isot.* **1989**, *40*, 715.
(142) Faller, P.; Ctortecka, B.; Tröger, W.; Butz, T.; Vasak, M. *J. Biol. Inorg. Chem.* **2000**, *5*, 393.
(143) Tröger, W.; Ctortecka, B.; Faller, P.; Butz, T.; Vasak, M. *J. Inorg. Biochem.* **1999**, *74*, 318.
(144) Kumar, V.; Kawaldeep; Singh, K. *J. Radioanal. Nucl. Chem. Lett.* **1992**, *166*, 131.
(145) Binarh, H. S.; Singh, H.; Ghumman, S. S.; Sahota, H. S. *J. Radioanal. Nucl. Chem. Lett.* **1990**, *146*, 75.
(146) Singh, H.; Binarh, H. S.; Sahota, G. P. S.; Sahota, H. S. *J. Radioanal. Nucl. Chem.* **1992**, *163*, 385.
(147) Martin, P. W.; Kalfas, C. A. *Nucl. Instrum. Methods* **1980**, *171*, 603.
(148) Ceolin, M.; Martinez, J. A.; Ermacora, M. R. *J. Biochem. Biophys. Methods* **1997**, *35*, 135.
(149) Ceolin, M. *J. Biochem. Biophys. Methods* **2000**, *45*, 117.
(150) Ctortecka, B.; Tröger, W.; Mallion, S.; Butz, T.; Hoffmann, R. *Hyperfine Interact.* **1999**, *121*, 737.
(151) Tröger, W.; Lippert, C.; Schmidt, P.; Schmidt, U.; Butz, T.; Hoffmann, R.; Zeppezauer, M. *Z. Naturforsch., Sect. A: Phys. Sci.* **1996**, *51*, 427.
(152) Martin, P. W.; Kalfas, C. A.; Skov, K. *Chem. Phys. Lett.* **1978**, *57*, 279.
(153) Butz, T.; Lerf, A.; Huber, R. *Phys. Rev. Lett.* **1982**, *48*, 890.
(154) Danielsen, E.; Bauer, R.; Schneider, D. *Eur. Biophys. J.* **1991**, *20*, 193.
(155) Hargrave, P. C.; Smith, F. A.; Bown, K.; Carr, R. *Chem. Phys. Lett.* **1995**, *246*, 626.
(156) Ma, W. L.; Hwang, K. J.; Lee, V. H. L. *Pharm. Res.* **1993**, *10*, 252.
(157) Schubert, R.; Joos, M.; Deicher, M.; Magerle, R.; Lasch, J. *Biochim. Biophys. Acta* **1993**, *1150*, 162.
(158) Kalfas, C. A.; Sideris, E. G.; Martin, P. W. *J. Appl. Radiat. Isot.* **1984**, *35*, 889.
(159) Liu, Y. F.; Qu, T.; Wang, X. Y. *Pure Appl. Chem.* **1991**, *63*, 1298.
(160) Martin, P. W.; El-kateb, S.; Kuhnlein, U. *J. Chem. Phys.* **1992**, *76*, 3819.
(161) Sideris, E. G.; Kalfas, C. A.; Katsaros, N. *Inorg. Chim. Acta Bioinorg. Chem.* **1986**, *123*, 1.
(162) Matzapetakis, M.; Farrer, B. T.; Weng, T. C.; Hemmingsen, L.; Penner-Hahn, J. E.; Pecoraro, V. L. *J. Am. Chem. Soc.* **2002**, *124*, 8042.
(163) Tröger, W. *Hyperfine Interact.* **2001**, *136*, 673.
(164) Heinz, U.; Bauer, R.; Wommer, S.; Meyer-Klaucke, W.; Papamichael, C.; Bateson, J.; Adolph, H. W. *J. Biol. Chem.* **2003**, *278*, 20659.

CR030030V